Università degli Studi di Ferrara

Dottorato di ricerca in Fisica
Ciclo XXIV

Coordinatore Prof. Filippo Frontera

Radiocarbon dating for contemporary art: hardware developments and measurements

Settore scientifico disciplinare FIS/07

Dottoranda:
Caforio Lucia Anna

Tutor interno:
Prof. Calabrese Roberto

Tutor esterni:
Prof. Petrucci Ferruccio
Dott.ssa Fedi Mariaelena

Anni 2009/2011

Contents

Introduction

The research developed during my PhD can be inserted within the activities of the Archaeometry Laboratory of the Ferrara Physics Department. In this laboratory, the artworks of historical-artistic interest are studied using non invasive and non destructive methods for diagnostic purposes and for a support to the work of the restorers, in order to identify e.g. the executive technique and the pigments utilized by the artists. In more recent years, the same methods have been also applied to investigate contemporary paintings (typically dated back to the period since the end of the 19^{th} century until present). In fact, a rising interest has concerned this kind of artworks, given the necessity to characterize the new used materials to preserve these works of art by the natural and fast deterioration.

In addition, concerning contemporary art, it is well known that an important aspect, mainly in the trade field, is the authentication and so the identification of fakes. A simple analysis of the artistic style cannot sometimes be sufficient to solve these issues, while the support of scientific analyses, like that provided by a robust dating technique, is often required. In this framework, during my PhD, the capability to solve authentication issues by radiocarbon dating in an univocal way has been tested.

Radiocarbon (^{14}C) is surely the principal radiometric method to study the past and in particular to date organic archaeological findings. However, since the end of the 1960s, radiocarbon has been also applied to forensics, initially in biological and medical fields, but also in archaeometry to identify forgeries of ancient artworks. The possibility to use ^{14}C for the most recent samples is given by the so-called Bomb Peak. By this expression, the huge increase of the radiocarbon concentration in atmosphere after the Second World War is usually addressed. Actually, in the late 1950s and early 1960s, as a consequence of hundreds of nuclear weapon tests, large amounts of neutrons were produced in the atmosphere, thus significantly increasing the radiocarbon production rate. This artificial ^{14}C input caused not only a global increase of the $^{14}C/^{12}C$ ratio in the atmospheric CO_2 but also in all the other reservoirs, i.e. in the oceans and in the biosphere. The increase was so large that the atmospheric radiocarbon concentration was almost doubled in less than 10 years. Then, after 1963, when the Nuclear Non-Proliferation Treat was signed, the ^{14}C concentration started to

decrease due to the rapid exchanges with the carbon reservoirs. This is just the peculiar trend of the ^{14}C concentration that is exploited in forensics to date samples with a very high precision.

During my PhD, to verify the possibility to date by radiocarbon contemporary artworks showing advantages and limits of the method, I have measured the ^{14}C abundance in many paper and canvas samples of the 20th century. These materials were chosen because they represent the most common supports for artworks. All the samples were also carefully analysed by other techniques (Scanning Electron Microscopy, Fourier Transform Infrared Spectroscopy and Attenuated Total Reflectance Spectroscopy) to study the raw materials and their state of preservation, allowing us to choose the better protocol for the sample preparation (i.e. all the procedures to convert any sample to be dated to the proper chemical form needed for the measurements).

All the radiocarbon measurements were performed by Accelerator Mass Spectrometry (AMS) at INFN-LABEC (*Laboratorio di Tecniche Nucleari per i Beni Culturali*) in Florence, where a 3 MV Tandem accelerator is installed. Sample preparation to convert the samples to the graphite pellets for the AMS measurements was performed at LABEC as well. During my PhD, I have been also involved in the upgrade of the experimental set-up.

In the first chapter of this thesis, the basic principles of radiocarbon dating are described; in particular, the attention is focused on the natural and the anthropogenic causes that have affected the radiocarbon concentration in all living organisms during the centuries. In brief, the main reasons of the use of Accelerator Mass Spectrometry to perform radiocarbon measurements are also discussed.

In chapter 2, the features of AMS are described in detail. First, the standard sample preparation procedure (pre-treatment, combustion and graphitization process) necessary to obtain a graphite sample to be measured is presented. In particular, the need of the pre-treatment is due to the presence of possible contaminations in the sample to be dated; the specific case of contamination by dead carbon is mentioned, since this is the case that can be found when dealing with contemporary art samples. The 3 MV Tandem accelerator installed at LABEC is also explained; the AMS beam line is shown with reference to radiocarbon measurements.

In chapter 3, all the improvements in the experimental set-up developed during my PhD are presented. The new graphitization line and the upgrades of the AMS beam line are

described. Concerning new chemical pre-treatments, the new alpha cellulose extraction procedure and the new chloroform-based protocol for restored samples are reported.

In the fourth chapter, the radiocarbon measurements performed on paper and canvas samples of the 20th century are shown. Thanks to these measurements, the advantages and the limits of radiocarbon dating are highlighted.

In the last chapter, two case studies that demonstrate the feasibility of using radiocarbon dating applied to art are presented. The first case concerns the application of the new chloroform-based pre-treatment on a restored painting; as for the second case study, the identification of a forgery of a contemporary artwork is shown.

Chapter 1
Radiocarbon dating

In the mid of 1940s, studying the effects of cosmic rays on the earth and the earth's atmosphere, Willard Libby put the bases of a new dating method based on the measurement of the residual abundance of a cosmogenic isotope: ^{14}C (or radiocarbon). For this research, in 1960, he received the Nobel Prize in chemistry. Nowadays, radiocarbon dating represents one of the most important techniques to investigate the past. It has been used especially by archeologists to study the human evolution, but it has been also applied to others fields, such as geology, biology, art and forensics. In this chapter, the basic principles of radiocarbon dating are discussed.

1.1 Basic principles

Carbon is one of the most abundant elements on earth. In nature, there are three natural carbon isotopes. ^{12}C and ^{13}C are both stable and correspond to the 98.9% and 1.1% of the carbon on earth, respectively. ^{14}C is present in a very small concentration and it is the only unstable isotope. It decays via beta emission to ^{14}N with a half life $T_{1/2}$ = 5730±40 years [God1962].

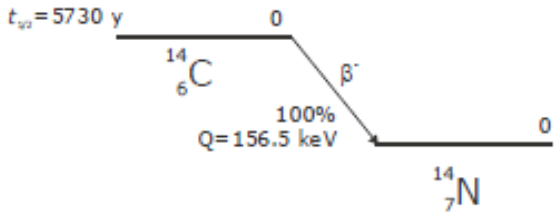

Fig 1.1 Scheme of the radiocarbon decay.

^{14}C is produced in the upper layers of the atmosphere by interaction of thermal neutrons (secondary products of cosmic rays) and nuclei of nitrogen:

$$^{14}N(n,p)^{14}C \tag{1.1}$$

^{14}C atoms rapidly combine with oxygen to form carbon dioxide. Considering the radiocarbon half life and its fast production rate, the decayed radiocarbon is promptly compensated by natural continuous production; in this way, the ^{14}C concentration in atmosphere can be considered constant, of the order of $1.2 \cdot 10^{-12}$. Moreover, CO_2 spreads over the atmosphere and dissolves into the oceans. It enters also in the biosphere via e.g. photosynthesis in plants and nutrition in animals. A dynamic equilibrium is established between living organisms and the environment where they live, so that in all of these organisms the same ^{14}C concentration as in the atmosphere is present.

When an organism dies, if we can consider it as a close system, this concentration starts to decrease due to radioactive decay. Assuming that the radiocarbon concentration in atmosphere has been constant in the past and it is the same in terrestrial and marine organisms, the residual radiocarbon concentration $^{14}R(t)$ after a period t from the death is in agreement with the radioactive law:

$$^{14}R(t) = \frac{^{14}C}{C_{total}} \approx \frac{^{14}C}{^{12}C} = {}^{14}R_0 \cdot e^{-\frac{t}{\tau}} \tag{1.2}$$

In the equation (1.2), $^{14}R_0$ is the radiocarbon concentration at the moment of death and τ is the ^{14}C mean life (= $T_{1/2}/\ln 2$). Adopting for $^{14}R_0$ the conventional value of $1.2 \cdot 10^{-12}$, i.e. the radiocarbon concentration in atmosphere in a year chosen as reference, namely AD 1950, and for τ the value of 8033 years (the so-called Libby mean life), we can define the conventional radiocarbon age t_{RC} as:

$$t_{RC} = \tau \cdot \ln\left[\frac{^{14}R_0}{^{14}R(t)}\right] \tag{1.3}$$

The conventional radiocarbon age is expressed in years Before Present (years BP), where Present is 1950. 1950 was chosen as reference year partly for historical reasons (in that period, the first experimental results were published), but also because after this year the atmospheric radiocarbon concentration started to considerably change due to nuclear weapon

tests (see paragraph 1.3.2).

The age obtained from the equation (1.3) is not the true age of the sample, because some of the assumptions used to calculate t_{RC} are true only as a first approximation (e.g. the hypothesis according to which radiocarbon concentration in atmosphere has been constant in the past and it is equal in all organisms). In the next paragraphs these assumptions are discussed.

1.2 Variations of ^{14}C in living organisms

When the conventional radiocarbon age (1.3) is defined, it is supposed that all living organisms are characterized by the same ^{14}C concentration as the atmosphere. Actually, there are some alteration effects, depending on different carbon uptake paths and the environment where the organisms live, that may affect the radiocarbon concentration. The principal consequence of these effects is a discrepancy between the measured ^{14}C concentration and the expected value.

One of the most important effects is known as isotopic fractionation, which is characteristic of many biological and chemical processes in which the isotopes of the same element are assimilated in different ways by living organisms; in particular, the lightest isotopes are preferentially taken up. In the case of processes involving the carbon isotopes, this means that ^{12}C is better absorbed than ^{13}C and ^{14}C by the growing plants or animals. If the measured ^{14}C concentration in a sample is very different with respect to the atmospheric value, the dated organisms will appear to be older or younger. In order to correct this effect, being ^{14}C radioactive, the $^{13}C/^{12}C$ ratio is measured in all samples, since these two isotopes are stable and the variations of their abundances can be attributed only to fractionation.

The fractionation of ^{13}C relative to ^{12}C in a sample is defined as

$$\delta^{13}C = \left[\frac{\left(^{13}C/^{12}C\right)_{sample} - \left(^{13}C/^{12}C\right)_{VPDB}}{\left(^{13}C/^{12}C\right)_{VPDB}} \right] \times 1000 \qquad (1.4)$$

where $(^{13}C/^{12}C)_{sample}$ and $(^{13}C/^{12}C)_{VPDB}$ are respectively the isotopic ratio in the sample and in the standard *VPDB* (Vienna Peedee Belemnite), a limestone fossil from a crustaceous formation in South Carolina (USA) [Cop1994]. Assuming the relationship between ^{13}C

fractionation and ^{14}C, demonstrated in [Cra1954], it is possible then to correct the measured $^{14}C/^{12}C$ ratio:

$$\left(\frac{^{14}C}{^{12}C}\right)_{sample,corr} = \left(\frac{^{14}C}{^{12}C}\right)_{sample,meas}\left(1-2\frac{25+\delta^{13}C_{sample}}{1000}\right) \qquad (1.5)$$

In the equation (1.5), by international convention, the $\delta^{13}C_{sample}$ baseline is fixed at -25‰ with respect to *VPDB*; this value corresponds to the mean isotopic fractionation of terrestrial wood.

In Figure 1.2, the $\delta^{13}C$ of several materials are reported.

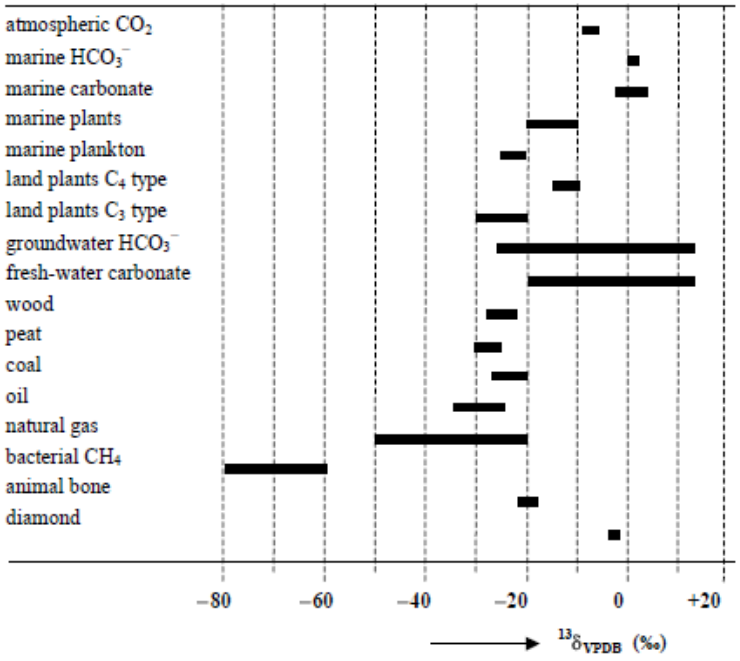

Fig 1.2 Overview of isotopic fractionation mean values in different natural compounds (reproduced from [wIA2011].

An effect concerning marine organisms is the so-called reservoir effect. In the oceans, the atmospheric carbon dioxide is exchanged only on the surface layers of water, which are so rich in ^{14}C. Then, thanks to marine flows, CO_2 absorbed from the atmosphere can diffuse into the deep waters. In the meantime, the upwelling mechanism contributes to mix the waters, moving upwards the "old" waters, depleted in radiocarbon, and thus diluting the ^{14}C concentration present in the ocean surface. Hence, as effect of these processes, the marine

samples are characterized by a lower radiocarbon concentration than terrestrial samples, showing a typical apparent ageing of about 400 years (as an average).

1.3 Variations of ^{14}C in atmosphere

In order to test the new radiometric dating method, Libby performed the first measurements on samples of known ages, in particular archaeological findings from ancient Egypt. During the 1950s, when the instrumental set ups (in particular, the detection systems) and so the accuracy of the measurements improved, a discrepancy between the measured radiocarbon ages and the historical Egyptian chronology was eventually noticed [Lib1960, Bow1990]. This fact could be explained by assuming a variation of the ^{14}C concentration in atmosphere during the centuries, as it was verified by measuring the radiocarbon content in samples that could be dated also by independent methods, i.e. tree rings.

Trees grow up annually, usually adding a single ring to their trunk each year. This ring is the only one that exchanges carbon with the atmosphere, reaching an equilibrium condition; thus it stores the ^{14}C concentration of the year in which it "lived". In this way, the measurements of ^{14}C concentrations in tree rings allow recording the atmospheric variations year by year. A calibration curve, in which measured radiocarbon ages are correlated to calendar ages, can be so arranged, by comparing the radiocarbon data to the dates obtained by independent method e.g. dendrochronology[1]. In fact, the first recommended calibration curve, which covered the time period BC 2500 – AD 1950, was obtained by combining radiocarbon ages with dendrochronologically dated wood [Pea1986, Stu1986]. Since then, new materials have been dated, now extending the calibration curve back to about 50.000 years BP; these materials are corals, foraminifera and varve lake sediments, dated by other independent methods, such as that based on Uranium/Thorium series. In Figure 1.3, a portion of the recently updated calibration curve, IntCal09, is shown [Rei2009].

[1] Dendrochronology is a dating method based on the analysis of patterns of tree rings. Measuring e.g. the width and the density of tree rings, master chronologies for different trees species are obtained. Therefore, comparing the sample rings with the corresponding master chronology, an absolute dating of wooden samples is achievable.

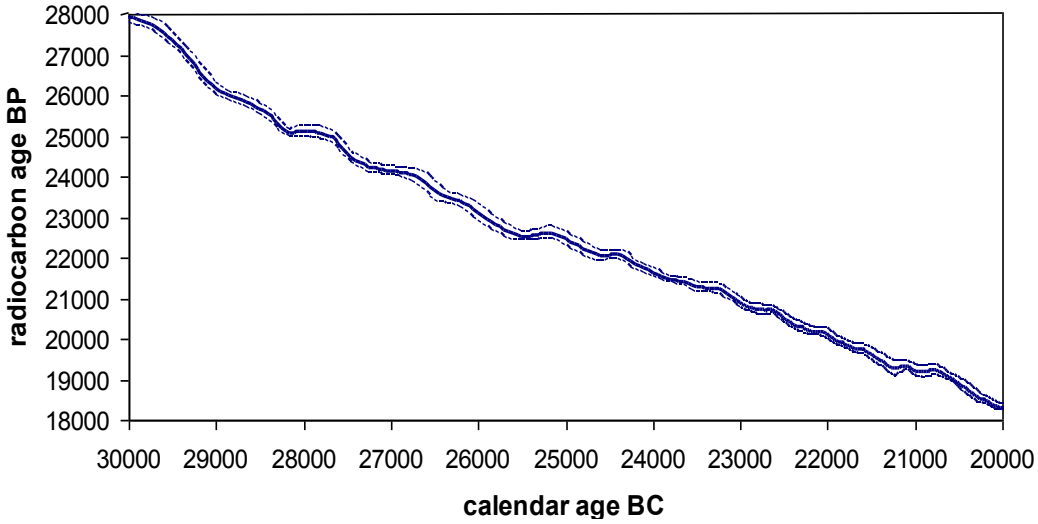

Fig 1.3 Portion of IntCal09, the atmospheric calibration curve [Rei2009]. On the y axis the radiocarbon age, expressed in years BP, and on the x axis the calendar age are reported.

Observing the Figure 1.3, we can notice that the calibration curve is not a monotonic function and it has not a constant trend.

1.3.1 Natural causes

The measured variations of the ^{14}C concentration in atmosphere are due both to natural and to anthropogenic causes that are described in the following.

Radiocarbon production in atmosphere is affected by the earth magnetic field, which is latitude dependent. Indeed, being charged particles, cosmic rays are deflected by magnetic field; as a consequence, the production rate of ^{14}C atoms on earth is not constant with the latitude; for example, a bigger ^{14}C concentration is present at the poles than at equator. This effect is minimized by a rapid mixing in the atmosphere due to the air fluxes that lead to uniform the ^{14}C concentration [Kor1980, Bow1990].

However, changes of the magnetic field in the past, such as reversals and polarity excursions, have strongly influenced the abundance of radiocarbon in atmosphere. The relationship between the magnetic dipole moment changes and the ^{14}C activity has been demonstrated by several investigators [Ste1983], finding a predominant trend with a periodicity of about 8000 years.

In addition, other short-term variations of the radiocarbon concentration are due to the solar activity. Actually, the variation of the solar activity causes a change of the flux of

protons on earth. Following this process, the quantity of neutrons, responsible of the ^{14}C atoms production, is not constant; thus, the radiocarbon production rate is variable with time. This effect was demonstrated in several studies [Kor1980, Sue1986, Der1995], just measuring the ^{14}C concentration in tree rings, as also explained in the previous paragraph. Generally, the solar variations have a periodicity of about 200 years and cause the so-called wiggles (fluctuations over short term calendar length). An 11-year sunspot activity cycle is registered too, but its effect has been estimated unimportant [Sue1986].

1.3.2 Anthropogenic causes

^{14}C variations in atmosphere have been caused not only by nature, but also by human activity, i.e. principally by the industrialization process and by the nuclear weapon tests.

Since the beginning of the 19th century, the continental Europe, in particular Germany and England, has been involved in the industrial revolution process. Appreciable amounts of carbon dioxide began to be added to the atmosphere thanks to the combustion of fossil fuel [Rev1957]. The rate of combustion has continuously increased causing a dilution of the natural radiocarbon concentration in the atmosphere and, as a consequence, a decreasing of the $^{14}C/^{12}C$ ratio in all carbon reservoirs (e.g. oceans) and in all living organisms. This effect was discovered by Hans Suess in 1953 [Lev1989]. In order to estimate this so-called Suess effect, measurements were performed again on tree rings [Aws1986, Paw2004]. The industrialization process has been not concluded yet, so that this effect is still present in all living organisms [Lev2000].

Another anthropogenic effect is known as Bomb Peak (or Bomb Spike). In the late 1950s and early 1960s, as a consequence of hundreds of nuclear weapon tests, large amounts of neutrons were produced in the atmosphere, thus significantly increasing the radiocarbon production rate. This artificial ^{14}C input caused not only a global increase of the $^{14}C/^{12}C$ ratio in the atmospheric CO_2 but also in all the other reservoirs (mainly the oceans and the biosphere). The increase was so large that the atmospheric radiocarbon concentration was almost doubled in less than 10 years. After 1963, when the Nuclear Non-Proliferation Treaty was signed [wFa2011], the ^{14}C concentration started to decrease due to the rapid exchanges with the carbon reservoirs. In Figure 1.6, the atmospheric radiocarbon concentration is reported as a function of the year: the huge increase starting since 1955 is evident. In the figure, four different curves are shown, each of them related to a defined region of earth.

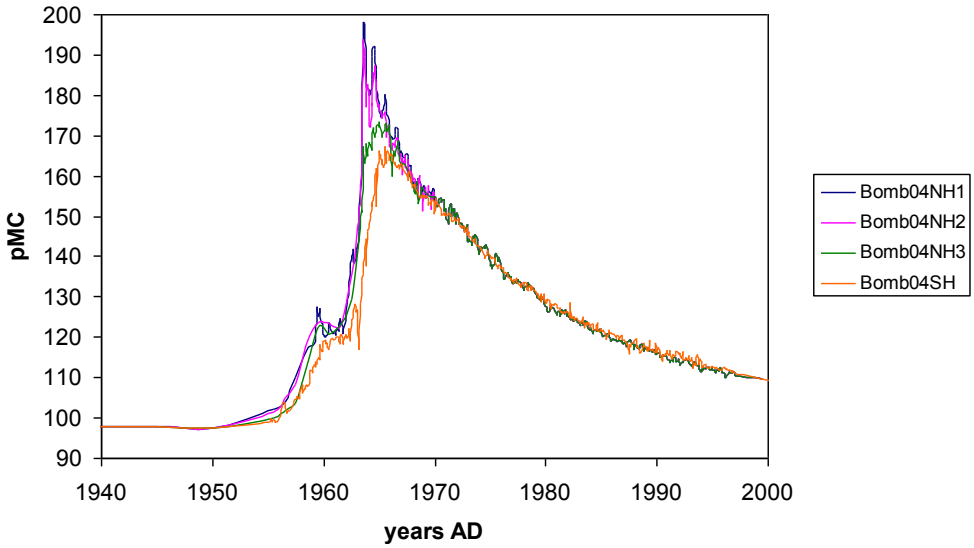

Fig 1.6 Atmospheric ^{14}C curves relative to the four zones of earth. The ^{14}C concentrations are expressed in pMC; reproduced from [Hua2004].

The NH1 zone covers the area from ~40°N to the North Pole; it is the zone where Italy (except the Sicily) is included. The NH2 zone extends from ~40°N to the summer maximum position of the summer so-called Intertropical Convergence Zone (ITCZ[2]); the NH3 zone covers the area from ITCZ to the equator; the SH zone is referred to the Southern hemisphere (see Figure 1.7).

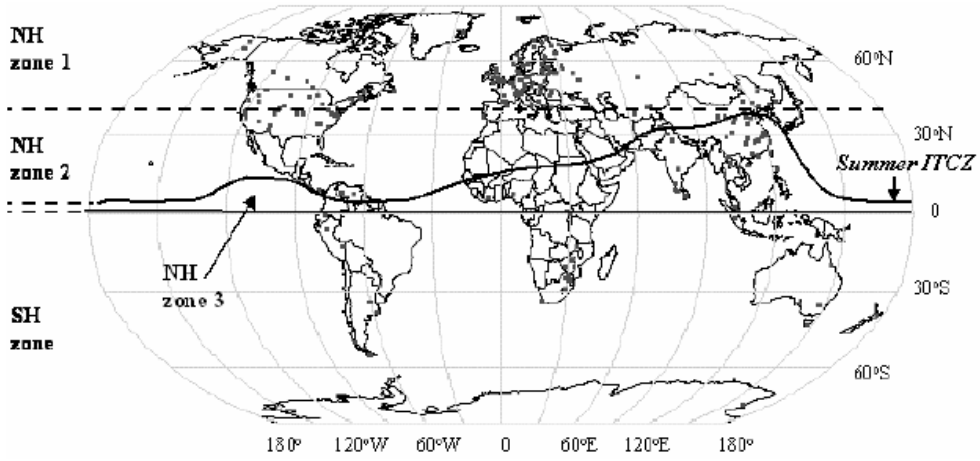

Fig 1.7 World map showing the four zones; reproduced from [Hua2004].

Slight differences in the radiocarbon concentrations in atmosphere among the four different zones can be noticed in Figure 1.6. The highest ^{14}C level was registered in northern

[2] ICTZ (Intertropical Convergence Zone) is a zone close to the Equator where winds originating in the northern and in the southern hemispheres come together.

mid to high latitudes, while in the subtropics and mid-latitudes the level was lower. Nevertheless, the major number of nuclear weapon tests was carried out in the Pacific Ocean at different latitudes. Probably, these differences can be due to a bigger ocean surface in the southern hemisphere, contributing to a shorter residence time of ^{14}C in the atmosphere than in the northern hemisphere.

The characteristic trend of the bomb peak curve allows us to date samples with a very high precision and permits thus the use of radiocarbon dating for forensics applications, for instance in biology and medicine to study the reproduction rate of the cells [Tun2004, Wil2000, Zop2004]. The Bomb peak curve can also be a very useful instrument in archaeometry, and in particular to recognize fakes of ancient artworks [Kre2004]. This PhD work has risen from the idea to use the bomb peak to also investigate contemporary artworks, realized in the 20th century. In the literature, not many applications on this topic are reported [Kei1972, Zav2004]. The advantages and the limits of using radiocarbon for such purposes are presented in this thesis, where measurements performed on different materials collected from objects of artistic interest of the 20th century are shown.

1.4 How to perform radiocarbon measurements

Only organic samples can of course be dated by radiocarbon. Among all the materials, we can here mention bone, charcoal, wood, textile, paper and papyrus. These samples generally are of archaeological and of historical-artistic interest. Since the radiocarbon dating method requires that a sample has to be collected from the object to be dated, the importance of choosing a measurement technique that needs just a small quantity of sample is mandatory. During the time, different methods for radiocarbon dating have been tested. The first measurements were done using the β counting method. Although this technique is not relatively very expensive and allows performing the measurements quite easily, a not positive aspect is the fact that it requires samples that are quite big. On the contrary, considering the typical historical value of the objects to be measured, the necessity to take a small sample is fundamental.

Nowadays, in most of the laboratories, radiocarbon measurements are performed using the technique known as Accelerator Mass Spectrometry (AMS) [Tun1998], which is based on the use of a particle accelerator coupled to selective filters like those characterizing a mass spectrometer.

In general, the basic principle on which mass spectrometry (MS) is based is that ions having the same energy and charge are deflected in a magnetic field with different trajectories according to their mass. The samples are ionized (usually as positive ions) and accelerated to energy in the range of 1-10 keV. Measuring the relative abundance of the isotopes, quantitative information about the sample can be obtained. In this range of energy the sensitivity is about 10^{-10}. Limitations to the sensitivity are also caused by the background counts, produced by interaction with apertures, walls and residual gas into the spectrometer [Fin1993].

Since the relative abundance of ^{14}C is only about $1.2 \cdot 10^{-12}$ (in modern samples) and the detection of this isotope is complicated by the presence of isobaric interferences that are more abundant than the ^{14}C itself, the typical sensitivity of traditional mass spectrometry is too low to permit the radiocarbon measurements. Indeed, concerning ^{14}C, one of the most important isobars is the stable isotope ^{14}N (see Figure 1.8), representing about 78% of the earth's atmosphere.

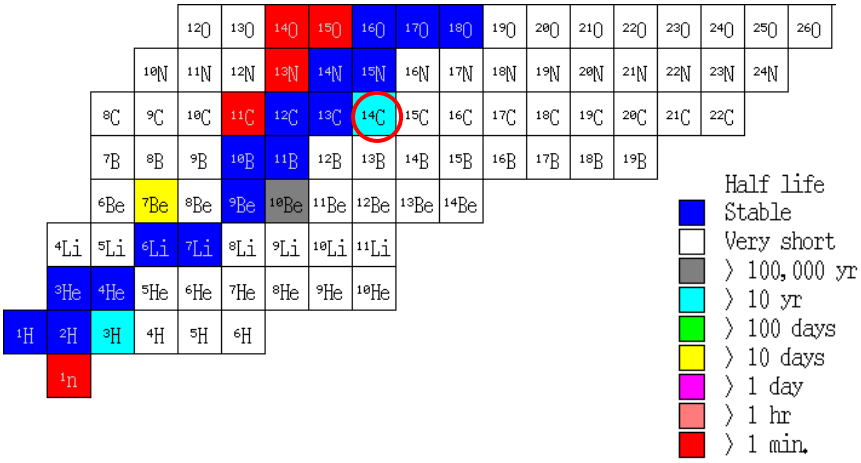

Fig 1.8 Portion of the table of nuclides showing carbon isotopes and their neighbours [wAt2000]

There are also molecular interferences. Indeed, ^{12}C and ^{13}C easily combine with H atoms, forming the $^{12}CH_2$ and ^{13}CH molecules; these molecules are characterized by a difference in masses extremely small.

The limits of traditional MS are overcome by Accelerator Mass Spectrometry. It represents a very useful method for radiocarbon measurements because:

- using a negative ion source, it is capable to suppress isobaric interferences that do not form negative ions (in the case of radiocarbon, the suppressed interference is ^{14}N);

- thanks to the stripping process at the high voltage terminal of the accelerator, the molecular interferences (i.e. $^{12}CH_2$ and ^{13}CH) are suppressed;
- working in a range of energies of the order of MeV allows identifying and separating the ions of interest from any residual atomic and/or isobaric interferences.

Thanks to these characteristics, AMS is able to reach a very high sensitivity (10^{-15}); in addition, the efficiency of the method allows measuring samples with masses of the order of few milligrams.

In chapter 2, the AMS technique applied to radiocarbon dating is described in details.

Chapter 2
Accelerator Mass Spectrometry

This chapter is divided into two sections. In the first part, the procedure to obtain a sample for ^{14}C-AMS measurements is explained; in the second part, the Tandem accelerator installed at INFN-LABEC (LAboratorio di tecniche nucleari per i BEni Culturali, Florence), where the measurements for this thesis were performed, is presented; in particular the AMS beam line is described.

2.1 Samples preparation for AMS measurements

With the term samples preparation, all the physical-chemical procedures used to treat the samples to be dated and the graphitization process employed to convert them into graphite (the chemical form for the sample to be inserted in the source of accelerator[3]) are meant. In particular, samples preparation aims at the removal of the contaminants that may affect the measurements and at the extraction of the suitable organic fraction to be dated.

The typical masses collected for a radiocarbon AMS measurement are of the order of some tens of mg (see Table 2.1), bigger than the mass of the final graphite pellet that will be used for the measurement itself (typically of the order of some hundreds of μg). Indeed, during the different steps of sample preparation, a mass loss has to be taken into account. This mass loss depends on the type of materials and on the percentage of contaminants present in the samples.

[3] For radiocarbon measurements, the most of the AMS facilities are equipped with ion sources for solid state samples. There are also hybrid ion sources that are able to measure also samples in a gaseous state. For instance, this type of sources is advantageous in measuring very small samples (about ~50μg) [Ruf2010].

Materials	Masses (mg)
Charcoal	20-40
Wood	20-30
Textile	30-40
Paper	20-30
Bone	1000

Table 2.1 Order of magnitude of the typical masses of collected samples for radiocarbon measurements for different materials (before any treatment).

2.1.1 The issue of contaminations and the extraction of the suitable fraction to date

In general, there are two different kinds of contaminations:

- contamination by "dead" carbon (e.g. carbonates)
- contamination by "modern" carbon (e.g. humic acids).

The term "dead" carbon is referred to all materials containing a ^{14}C concentration that is well below the sensitivity limit of the measurement technique, thus appearing infinitively old; as a consequence, if a percentage of this contamination is present in the samples, their radiocarbon age will appear older than the true age. In the case of "modern" carbon, the effect on radiocarbon age is opposite. Indeed, adding a contamination with a ^{14}C content equal to the present concentration in atmosphere, the measured samples will appear younger.

More specifically, the case of contamination by dead carbon is here explained, since this is the situation that may occur when dealing with dating findings of historical-artistic interest, such as those analysed in this thesis. The relationship between the measured radiocarbon concentration $^{14}R_{meas}$ and the fraction x of dead carbon contamination in the sample is:

$$^{14}R_{meas} = \frac{1}{1+x} \cdot {}^{14}R_0 \exp\left(-\frac{t_{true}}{\tau}\right) \tag{2.1}$$

where t_{true} is the true radiocarbon age. Therefore, the apparent radiocarbon age t_{app} is:

$$t_{app} = \tau \ln \frac{^{14}R_0}{^{14}R_{meas}} = t_{true} + \tau \ln(1+x) \qquad (2.2)$$

Hence, a dead carbon contamination of 1% introduces an absolute discrepancy on the measured radiocarbon age of 80 years. This contamination effect is independent of the true age of the sample, but, obviously, this effect is more significant for recent sample.

Contaminations can be natural and/or anthropogenic. The natural contaminations, such as traces of humic acids from the soil and of calcium carbonates dissolved in groundwaters, are especially characteristics of archaeological findings (i.e. bones, charcoals and seeds) that had been buried for several centuries. Being a non endogenous carbon fraction, these traces have to be removed to exclude any contamination effect on measured radiocarbon ages. As far as the anthropogenic contaminations are concerned, the materials and the chemical products used by restorers to consolidate historical objects can be taken into account. These products are usually obtained by industrial processes and are synthesized by hydrocarbons, which are obviously fossil carbon based. These products are thus sources of contamination by dead carbon and their incomplete removal can affect the measured radiocarbon age.

As introduced above, the other goal of the sample preparation is the extraction from the sample of the appropriate fraction to be dated. To illustrate this, the case of bone can be reported as an example. Bone is formed by two fractions: an organic fraction, consisting in the collagen protein (more subjected to degradation), and an inorganic fraction, essentially calcium hydroxyapatite ($Ca_5(PO_4)_3(OH)$). Both components contain carbon, so, in principle, both of them might be dated. In practice, the inorganic fraction can be contaminated by calcium carbonates originated from percolating groundwater; hence, in order to exclude the contribution of non endogenous carbon, this fraction is removed using a chemical pre-treatment and only the collagen is extracted and dated. Collagen is only a small fraction in bone. This is the reason of the use of about 1 g of bone samples to be treated [McC2010, Tal2011].

2.1.2 The “standard” sample preparation protocol

At INFN-LABEC, a sample preparation laboratory is present; here the samples are subjected to a standard protocol (pre-treatment, combustion, graphitization process). In this way, the samples are converted into graphite powder.

Initially the sample undergoes a physical treatment in order to remove the most external layers that might be more contaminated and might thus affect the radiocarbon dating. This operation generally consists in scratching the sample surface, using tweezers and a scalpel. If necessary, an observation under optical microscope can be useful.

Afterwards, the sample is treated with chemical reagents. The most suitable chemical protocol has to be chosen according to the sample material and to the fraction that we would like to extract and date. In most cases, a simple protocol, called ABA (acid-base-acid), is applied; it consists in a series of baths in acid and basic solution [wHi99]. The acid solution (typically, at LABEC, hydrochloric acid 1M) allows dissolving carbonate residues. The bath in alkaline solution (typically, at LABEC, sodium hydroxide 0.1M) has the role to eliminate humic acids. Finally, a further bath in acid is necessary to remove traces of atmospheric CO_2 entered in the solution in the previous step. The samples are then dried in oven.

Once the sample is clean, it is necessary to extract and isolate only carbon. For this purpose, the sample is oxidized so that carbon is collected as gaseous CO_2. At LABEC, this step is achieved by combusting the sample in an elemental analyzer (EA). The combustion process takes place in a furnace at a temperature of about 1100°C. The gas flows in a quartz column filled with different chemical materials (chromium oxide, reduced copper, silvered cobaltus oxide). As a consequence, when a typical organic sample is burnt, at the exit of this column, the gas is composed by N_2+CO_2+H_2O, while any sulphides are absorbed. Then, the three gaseous components pass through a gaschromatographic column, a spiral filled with an adsorbent material that adsorbs and desorbs the gases with different retention time according to their molecular weight. Therefore, the three gases come out of the column separately. At the exit of the gaschromatographic column, a thermal conductivity detector (TDC) is present. Three signals corresponding to each gas are detected. The area of each peak is proportional to the quantity of gas in the circuit. In Figure 2.1 a typical chromatogram acquired after gaschromatographic column is shown.

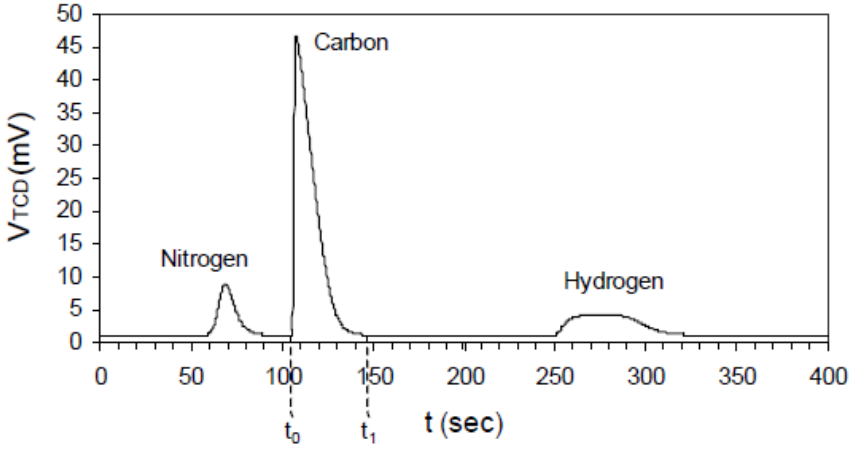

Fig 2.1 Chromatogram acquired for a cyclohexanone sample ($C_{12}H_{14}N_4O_4$): the three gaseous components are well time-separated.

During the time interval t_0-t_1 (see Figure 2.1), only the gaseous CO_2 is transferred into the graphitization line, where it is converted to graphite, exploiting the reaction:

$$CO_2 + 2H_2 \xleftarrow{Fe,600°C} C + 2H_2O \qquad (2.3)$$

In the reaction 2.3, carbon dioxide interacts with hydrogen at high temperature (about 600 °C) in the presence of iron powder as catalyst. The typical masses of the graphite samples prepared at LABEC (and for this work) are of the order of 700 µg. More details on the graphitisation line and on the principal steps of the graphitisation process will be given in chapter 3.

The iron and graphite mixture is then pressed into an aluminum target holder that is inserted in the source of the accelerator.

2.2 Accelerator Mass Spectrometry at LABEC

In the next paragraphs, the Tandem electrostatic accelerator installed at INFN-LABEC in Florence are explained. In particular, the AMS beam line will be described, with reference to radiocarbon measurements.

The 3 MV Tandem accelerator was produced by High Voltage Engineering Europe (HVEE) and it was installed in 2004 [Fed2007]. It is equipped to perform both AMS and Ion Beam Analysis (IBA) measurements.

In Figure 2.3 a schematic layout of the AMS beam line is shown.

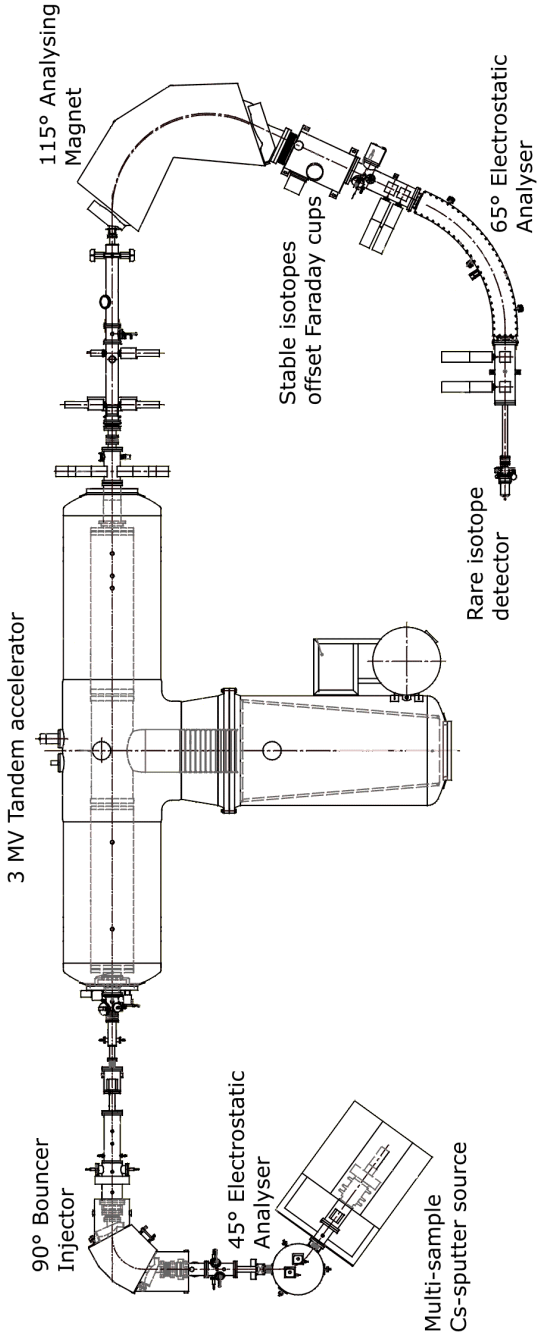

Fig 2.3 Schematic layout of the AMS beam line at the Tandem electrostatic accelerator of INFN-LABEC (the two other independent ion sources and the switching magnet to the beam lines dedicated to IBA measurements are not shown).

2.3 The Cs-sputter ion source

The ions injected into Tandem accelerators have a negative charge. The typical requirements for an AMS solid samples ion source are high stable currents, high efficiency, low memory effects, rapid sample switching and isobaric separation [Kil1997]. In particular,

- the high stable currents are important to reduce systematic errors especially when rare and abundant species are sequentially analyzed;
- the high efficiency is related to the possibility to measure very small samples;
- the low memory effect is necessary to guarantee the measurements in series of the samples minimizing cross contamination effects;
- the possibility to switch the samples can reduce the measuring time;
- the isobaric interferences due to particles that do not form negative ions can be suppressed.

The ion source installed on the AMS beam line at LABEC is of the Cs-sputter type.

As it is discussed in paragraph 1.4, the source acts as a filter to suppress the interference of nitrogen, since the nitrogen electron affinity is -0.07 eV.

In order to extract a negative beam from the sample (also called target), the graphite is bombarded by positive Cs ions. Cs is stored in a reservoir, which is heated up to about 75ºC; in this way, the vapours are released and come into contact with the spherical surface of the ionizer that is kept at about 1100 ºC. As a consequence of thermal ionization, positive Cs ions are formed. The Cs ions are accelerated on the sample surface thanks to a voltage of -7 kV (this voltage is called cathode voltage V_{cat}). The positive ions hit the sample graphite, sputtering atoms and molecules from the surface. Since the sample is cooled, a thin Cs layer is condensed on its surface, so that when the molecules and the atoms pass through this layer, they can acquire electrons, becoming negative. The most probable charge state is q=-1. Being the target at a negative potential with respect to ground (-35 kV), the ions are extracted from the source through the small central hole (~ 5 mm) of the ionizer. At the exit of the source, the energy E_{inj} of the negative ions is equal to E_{inj}=q(V_{ext}+V_{cat}), where q is -1, V_{ext} is the voltage difference between the ionizer and the exit of the source, kept at -28 kV, and V_{cat} is -7kV.

In Figure 2.4 the technical drawing of the source is reported.

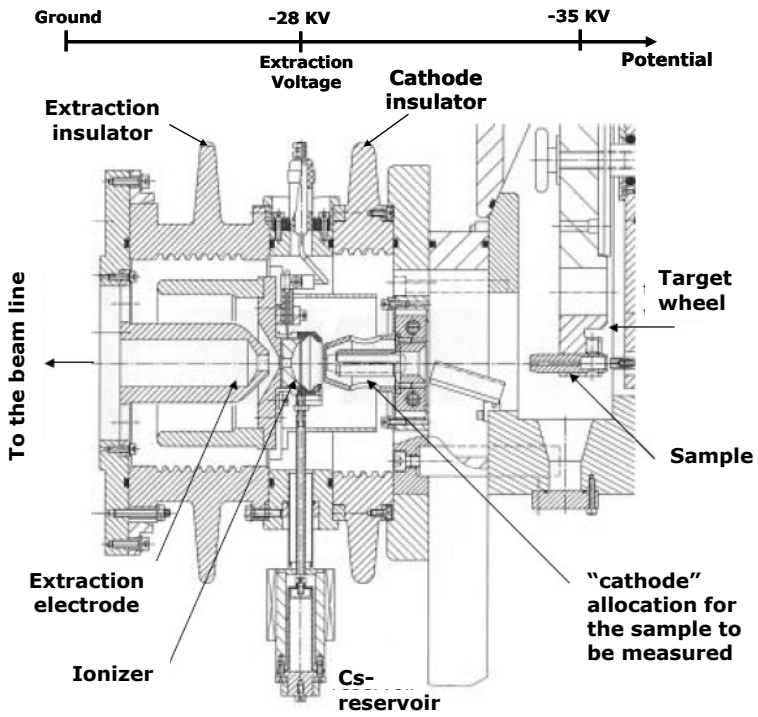

Fig. 2.4 Technical drawing of the Cs-sputter source installed at LABEC in Florence.

The source of the LABEC facility is equipped with a wheel, or a "carrousel", where up to 58 graphite samples pressed in the aluminium target holders can be allocated for the measurement (see Figure 2.5).

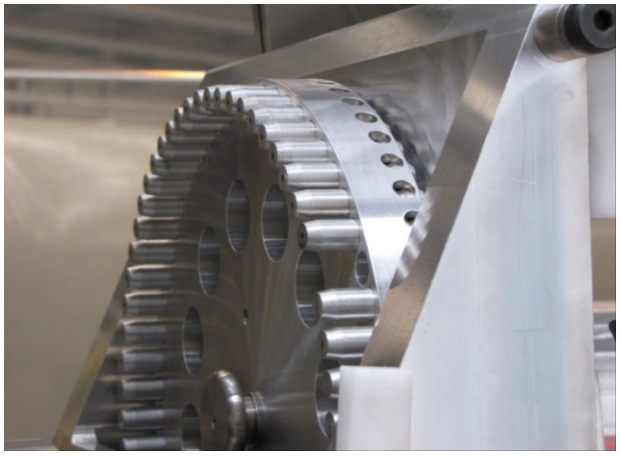

Fig 2.5 Picture of the wheel ("carrousel") with graphite samples ready for the measurement.

During the measurement, each sample is pushed in the sputtering position by a mechanical arm and then is moved with respect to the Cs beam in order to avoid the formation of a crater on the graphite surface. In our case, the sample is sputtered in 9 different positions.

2.4 Analysis on the low energy side

In Figure 2.6 a schematic layout of the elements present on the low energy side of the accelerator is shown.

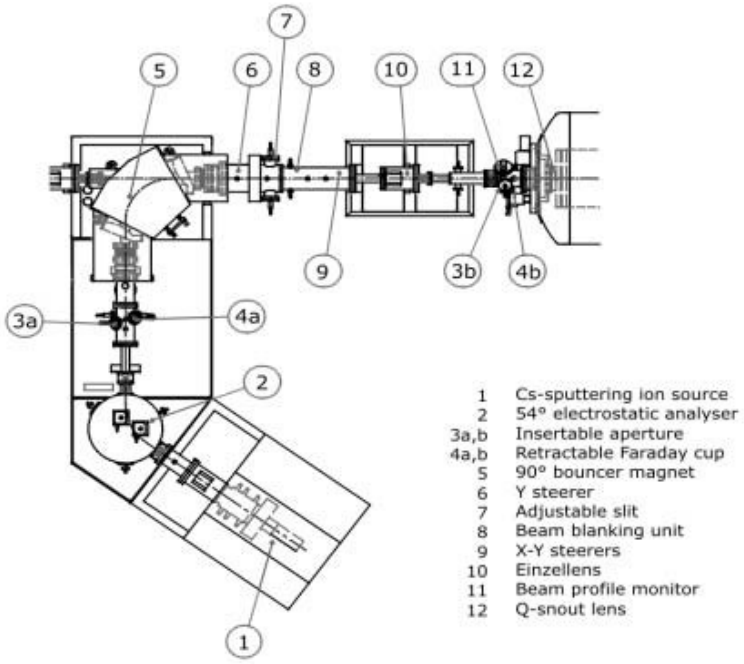

Fig. 2.6 Schematic layout of the low energy side on AMS beam line.

2.4.1 54° electrostatic analyzer

At the exit of the source, many fragments other than the ions that we would like to measure (^{14}C, ^{12}C and ^{13}C) can be present; if not correctly removed, they can represent interference during the measurements. In addition, the beam cannot be exactly monoenergetic. In order to analyze the beam, several filters are installed on the beam line after the source. The first is an electrostatic analyzer (ESA). It consists in two concentric cylindrical electrodes between which a potential difference is applied. The purpose of this filter is to select particles with a fixed ratio energy/charge (E/q). In fact, simplifying in the case of parallel electrodes, a defined E/q ratio can be selected according to:

$$\frac{E}{q} = \frac{r \cdot \varepsilon}{2} \tag{2.4}$$

where E and q are respectively energy and charge of the ions, ε is the electric field and r the radius of curvature of the filter. Considering that r is fixed by the construction geometry, changing the electric field, it is possible to select the ions of interest.

In this facility, the first ESA has a radius of 68.8 mm. The applied voltage of about 8 kV permits to select ions with charge -1 and energy 35 keV.

2.4.2 The injection magnet

A second analysis of the beam is performed by a 90° magnet that selects the ions according to the masses; in our case the masses to be selected are 12, 13 and 14.

In a magnetic field, ions of the same energy and charge state are deflected according to their masses:

$$r = \sqrt{\frac{2mE}{B^2 q^2}} \tag{2.5}$$

where r is the bending radius, B is the magnetic field, m, E and q are respectively mass, energy and charge of the ions.

Since r is fixed by the construction geometry, there are two possibilities to sequentially transmit the three masses of interest: changing the magnetic field or changing their energy. If we would like to quickly change the mass to transmit, the first method is not convenient since hysteresis effects can occur during the variations; hence, the best solution is to change the energy of the isotopes. To do this, the magnet is placed in a chamber that is electrically insulated with respect to the beam line. At its entrance, applying a proper voltage to the beam in rapid succession, we can change the energy of the ions so that the three masses can be injected into the accelerator one after the other (sequential injection).

In the AMS facility of LABEC, the field *B* in the magnet is set to transmit the mass 13; for the other masses the applied voltages are:

- $V_{bounc} \sim 2.9$ kV for 12
- $V_{bounc} \sim -2.5$ kV for 14.

Between the transitions, a “blanking” voltage is applied so that spurious particles are not introduced into the accelerator.

The typical time intervals to transmit the three masses in radiocarbon measurements are:

- Δt_{14}=8.5 ms
- Δt_{13}=0.6 ms
- Δt_{12}=6 μs.

Between Δt_{13} and Δt_{12}, a factor of 100 is chosen according to the natural isotopic ratio of the two isotopes; in this way, almost the same currents are measured for both.

At the exit of the magnet, the molecular interferences are still present. The beam is then injected into the accelerator, which also acts as a further filter.

2.5 The accelerator

In Figure 2.7 a picture of the tandem accelerator is reported.

Fig. 2.7 Picture of the tank of the Tandem accelerator at LABEC.

At LABEC, the high voltage is provided by a cascade generator similar to a Cockroft and Walton system[4]. The high voltage generator, the high voltage terminal and the accelerator tube are located in tank filled with an insulating gas (Sulphur Hexafluoride at a pressure of about 6 bar).

[4] In the Cockroft and Walton cascade generator, a radio frequency signal is capacitively coupled to a series of stacked diode circuits, which rectify the radio frequency and sum the signal to a high DC voltage [Fin1993].

The negative ions coming from the magnet enter into the accelerator. Here, they are accelerated to the high voltage terminal V_t (for radiocarbon measurements, V_t is kept at 2.5 MV), increasing their energy up to $E=E_{inj}+e\cdot V_t$, where E_{inj} is the energy of the ions at the entrance of the accelerator and *e* is the elementary electronic charge.

At the terminal, the ions undergo the stripping process. The stripping process is the losing of one or more electrons by the ion that interacts with matter. Loosing electrons, the ions change their charge state becoming positive. Once the equilibrium conditions are achieved, the most probable charge state depends on the terminal voltage.

In the LABEC facility, the Tandem accelerator is equipped with a gaseous stripper (Argon). The gas is recirculated by a turbo molecular pump in a tube of 13 mm diameter and 100 cm length; the pressure in the stripper canal can be estimated of the order of 10^{-2} mbar. With these features of the stripper gas and with a terminal voltage of 2.5 MV, the most probable charge state for carbon is 3+ (see Figure 2.8).

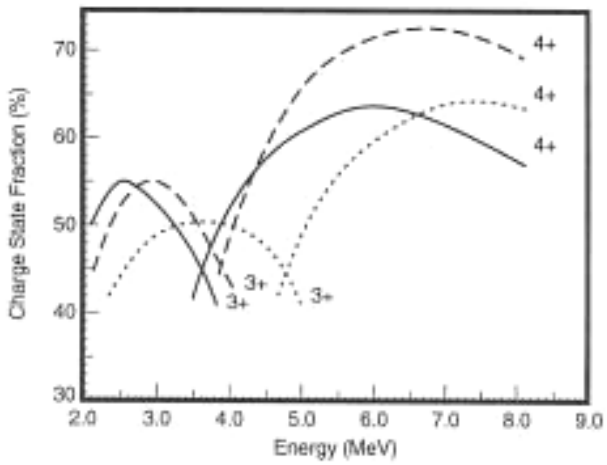

Fig. 2.8 Charge-state fraction of 3+ and 4+ ions of ^{14}C after stripping in O_2 gas (dotted line), Ar gas (dashed line) and carbon foil (full line). Reproduced from [Tun1998].

Another effect of the stripping process is the breaking of the molecular bonds. Analyzing a high charge state as 3+, a bigger probability to suppress the molecular interferences ($^{12}CH_2$ and ^{13}CH) is fulfilled.

After the stripping process, the positive ions beam is further accelerated to the ground potential. At the exit of the accelerator the energy of the ions is given by:

$$E_{fin} = (E_{inj} + e \cdot V_t) \cdot \frac{m_i}{m_{tot}} + qeV_t \qquad (2.6)$$

where E_{inj} is the energy of the negative particles before the injection, e is the elementary electronic charge, V_t is the terminal voltage, m_i is the mass of positive ions with charge state q and m_{tot} is the mass of negative injected ions. The energy of the carbon ions E_{fin} is about 10 MeV.

2.6 Analysis at high energy side

In Figure 2.9, a schematic layout of the elements present on high energy side is shown. As in the case of the low energy side, a magnet and an ESA filter are mounted in series.

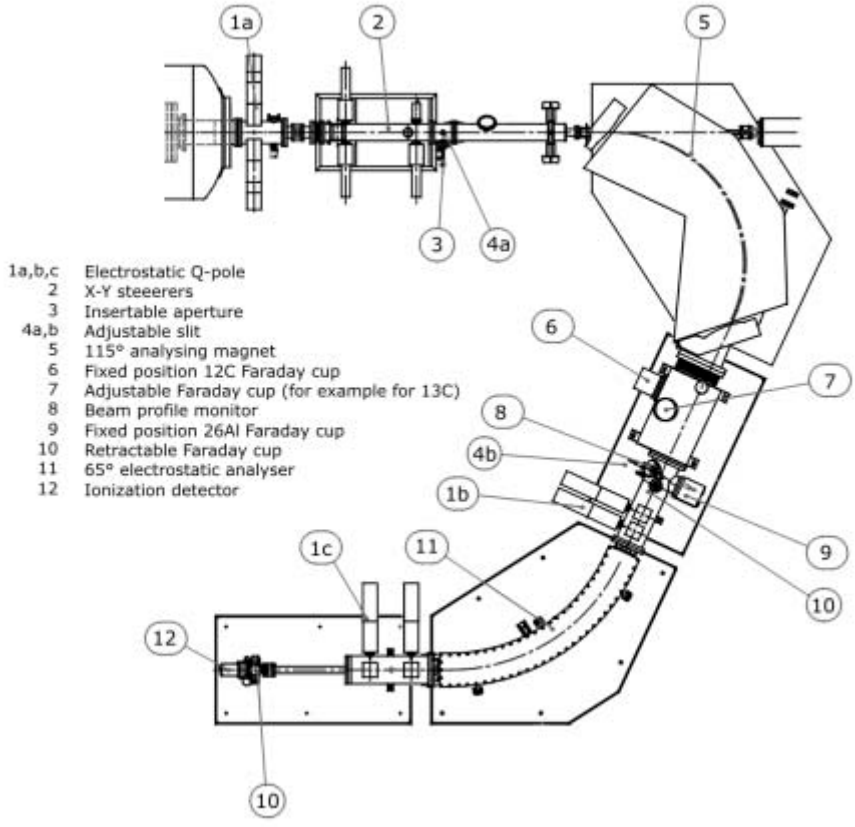

Fig. 2.9 Schematic layout of the AMS beam line on the high energy side.

The first selective element is the 115° magnet with a bending radius of 1.2 m. The magnetic field is set in order to transmit the $^{14}C^{3+}$ ions. The other two isotopes $^{12}C^{3+}$ and

$^{13}C^{3+}$, having the same energy and charge but different mass with respect to $^{14}C^{3+}$, cover different trajectories. They are colleted and measured by two offset Faraday cups just at the exit of the magnet. The measured currents for the two isotopes are, typically, of the order of 1-10 nA.

After the magnet, due to possible recombination and charge exchange processes in the accelerator tube, the beam might be still composed by various components having different energies and charge states. For instance, some particles might be involved in the stripping process not exactly at the terminal and thus might be accelerated to a different extent. In order to remove these possible interferences, ions with a fixed E/q value are then selected by a 65° electrostatic filter (ESA). This electrostatic filter is arranged with two cylindrical plates with a bending radius of 1.7 m and a gap of 40 mm. According to the formula 2.4, applying a potential difference of about 160 kV, ions with energy of 10 MeV and charge 3+ are selected, corresponding to the $^{14}C^{3+}$ ions.

2.7 Detection of the rare isotope ^{14}C

Since the counting rate of ^{14}C ions is too low to be detected by a Faraday cup, a detector used as a particle counter is installed. In fact, the typical count rate that we can expect in the case of a modern sample ($^{14}C/^{12}C \sim 10^{-12}$) is only about 15 s^{-1}. The signal coming from the detector is amplified and then acquired by a PC board in a spectrum only during the time interval Δt_{14} when the ^{14}C ions are injected into the accelerator.

In the first year of my PhD, the detector installed for radiocarbon measurements was a gas ionization chamber. The chamber was filled with ~25 mbar of butane (C_4H_{10}); the entrance window was a Mylar ($(C_{10}H_8O_4)_n$) foil with a diameter of about 10 mm and a thickness of 0.9 μm. The aluminium wall of the chamber acted as the cathode; while the anode was represented by an aluminium plate segmented in two parts for detection of the ΔE-E signal. In routine radiocarbon measurements, the information regarding the differential energy loss was not necessary and just the ΔE signal was typically acquired. In Figure 2.10, an example of a spectrum acquired for a modern sample is shown.

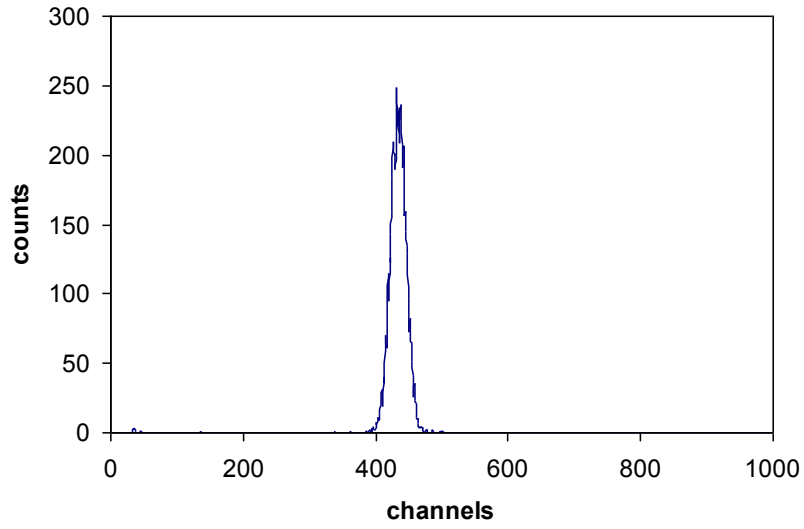

Fig. 2.10 Spectrum acquired for a modern sample.

2.8 Reporting ^{14}C data

In a routine radiocarbon measurement, unknown, primary and secondary standard and blank samples are inserted in the same carrousel. The primary standards, which are samples characterized by a certified radiocarbon concentration, are measured to normalize the $^{14}C/^{12}C$ isotopic ratio of the unknown samples; at LABEC, the so-called Oxalic Acid II (SRM 4990C), supplied by the US National Institute of Standard and Technology (NIST, formerly NBS) [Man1983], is used. The secondary standards are employed to test the accuracy of the ^{14}C measurement; for instance, at LABEC, samples from IAEA C7, supplied by the International Atomic Energy Agency[5], are usually prepared. Blank samples are characterized by a nominal ^{14}C abundance equal to zero or at least well below the sensitivity limit of an AMS measurement. Being combusted and graphitized using the same procedure of the unknown samples, they are used to verify whether some contaminations are introduced in the different preparation steps. They also allow estimating the intrinsic background of the accelerator during the measurement. The contribution of this background is then subtracted to the $^{14}C/^{12}C$ isotopic ratios measured for the unknown and standard samples. At LABEC, the blank samples are obtained from a synthetic material, cyclohexanone ($C_{12}H_{14}N_4O_4$).

As already discussed in paragraph 1.2, the $^{14}C/^{12}C$ isotopic ratios measured both in standards and unknown samples have to be corrected for the isotopic fractionation effect; to

[5] See paragraph 3.1 for details on the certified radiocarbon concentration.

do this, according to equation (1.5), $^{13}C/^{12}C$ isotopic ratios are also measured in the accelerator.

Finally, the measured radiocarbon concentration $^{14}R_{sample}$ in unknown samples is usually expressed as per cent of Modern Carbon (pMC), according to:

$$pMC(\%) = \frac{^{14}R_{sample}}{^{14}R_{ref}} \cdot 100 \tag{2.7}$$

where $^{14}R_{ref}$ is the 95% of the radiocarbon concentration measured in NBS Oxalic Acid I, supplied in 1950 by the National Bureau of Standards (NBS). Of course, in order to define pMC as a time-independent value, $^{14}R_{sample}$ and $^{14}R_{ref}$ have to be measured at the same time (or have to be time-corrected to be referred to the same measurement time).

Chapter 3
Hardware developments and new pre-treatment protocols

In this chapter, the developments and the improvements of the experimental set-up are presented. Two hardware developments, i.e. the new graphitization line and the new detector installed on the AMS beam line, and new chemical protocols to treat the samples before radiocarbon dating are discussed. For each of these improvements, the performed tests are shown.

3.1 The new graphitization line

In paragraph 2.1.2, a brief description of the standard protocol used to obtain a graphite sample to be measured by AMS is reported. During my PhD, the graphitization line at the LABEC laboratory was replaced. In Figure 3.1, a picture of the new line is shown.

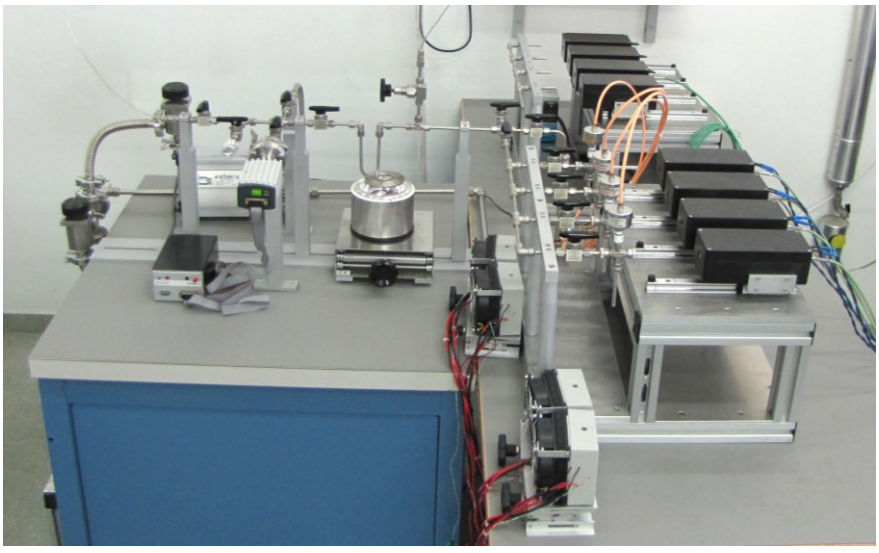

Fig. 3.1 Picture of the new graphitization line.

The new line was designed because, during the years, a slight increase of the pMC value in blank samples was noticed, as it is shown in Figure 3.2 where the average blank values measured during five years are reported. As it is said in chapter 2, the blank samples are characterized by a ^{14}C concentration nominally equal to zero or, at least, well below the sensitivity limit of AMS; hence, these samples give us the possibility to verify whether contaminations have been introduced during sample preparation and AMS measurement, estimating the background contribution (due to both sample processing and measurement in the accelerator). In fact, an increase of the pMC value measured in blanks corresponds to a decrease of the sensitivity achievable in the AMS measurements, putting a limit on the oldest sample that can be dated.

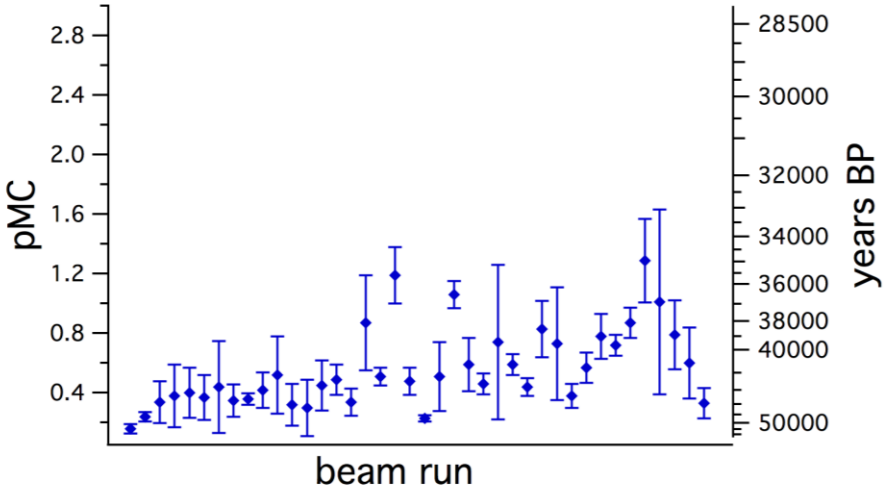

Fig 3.2 Average blank values measured since 2004 until 2009. Each point represents the average calculated over the several blanks measured in a same beam run; the quoted error corresponds to the maximum deviation. On the left y-axis the radiocarbon concentration, expressed in pMC, is reported; on the right y-axis the corresponding radiocarbon age expressed in years BP is shown.

The new graphitization line was thus thought in order to:

- improve the vacuum level in the line;
- reduce the effect of contamination possibly correlated to the graphitization process and to the deterioration of some mechanical components of the line.

The line (see Figure 3.3) was designed keeping the structure of the old graphitization line, adding some improvements:

- installation of a new Swagelok® three-way valve at the outlet of the elemental analyser (EA), in order to easily switch the gas flowing from the EA either into the line or into

atmosphere;

- substitution of the old LN_2 trap with a new spiral trap arranged in the horizontal plane in order to provide a homogeneous cooling in liquid nitrogen;
- addition of a new connection to transfer the CO_2 obtained from samples that are not combusted in the elemental analyzer[6];
- capability of installing up to eight graphitization reactors in order to have the possibility to prepare up to eight samples in parallel.

The schematic layout of the new graphitization line is presented in Figure 3.4.

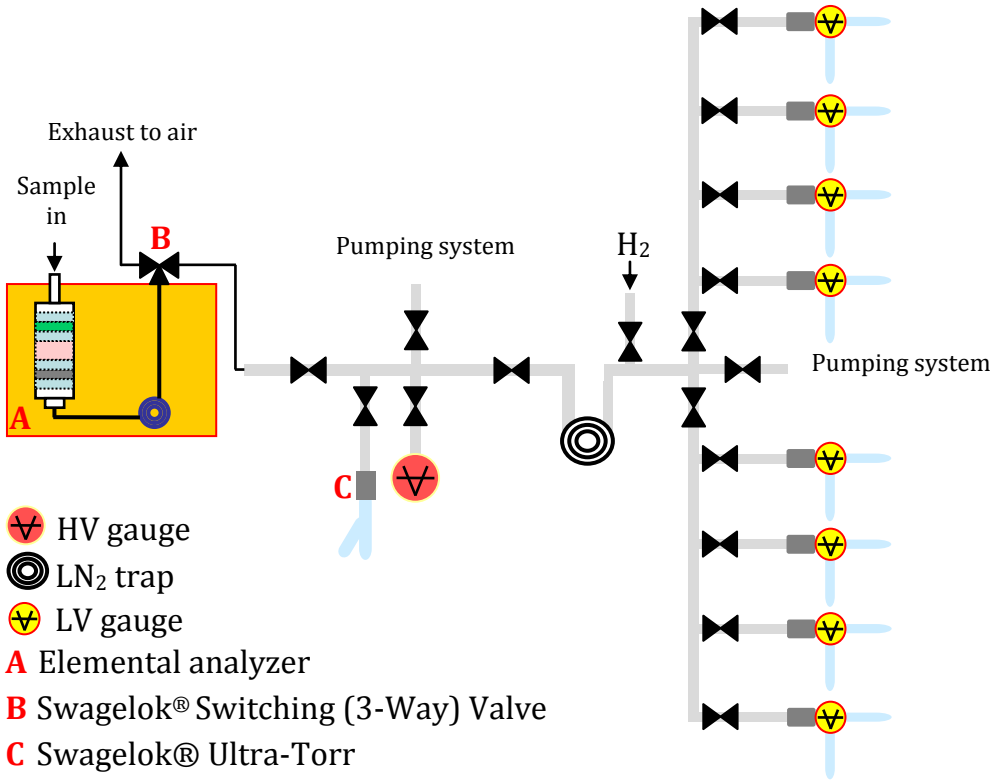

Fig. 3.3 Schematic layout of the new graphitization line.

Talking about how to operate on the line, the gaseous mixture of CO_2 and helium coming out from the elemental analyzer[7] is transferred to the graphitization line thanks to the new 3-way switching valve. The valve is switched to the line just in the moment when the CO_2 is flowing, i.e. when the correspondent peak is visible in the chromatogram. In the graphitization line, the gases

[6] For instance, carbonates (e.g. foraminifera and shells) can be either combusted using the EA or can undergo a chemical reaction ($3CaCO_3 + 2\ H_3PO_4 \rightarrow Ca_3(PO_4)_2 + 3CO_2 + 3H_2O$), which takes place in an independent dedicated preparation line.

[7] It is worth to remember that helium is used in the EA as carrier to transport the gases through the combustion and gaschromatographic columns and the gas detector.

are first collected in the freezing trap (LN_2 in Figure 3.3). Since helium does not condense at the LN_2 temperature, it can be removed by the pumping system[8] while carbon dioxide is kept frozen in the trap. Afterwards, when the helium is completely removed, the spiral is heated and CO_2 can be transferred to the quartz reactor where graphitization takes place. The quartz tube for the reaction has been already filled with iron powder that acts as catalyst in the graphitization (see equation 2.3). A double quantity of hydrogen with respect to the CO_2 is also added in the reactor in order to convert the CO_2 into elemental carbon, i.e. graphite (see the reaction described in paragraph 2.1.2, equation (2.3)). Since the reaction takes place at 600°C, the tube filled with iron is inserted in an oven. At the same time, the water, secondary product of the reaction, is trapped in order to prevent the reverse reaction to start. To this purpose, the other quartz tube of the reactor acts as a cool finger inserted in a Peltier cooling device (reaching a temperature of about -20°C). After about two hours and a half, the reaction is complete and the graphite sample is obtained. In Figure 3.4, the typical pressure trend of the graphitization reaction is shown.

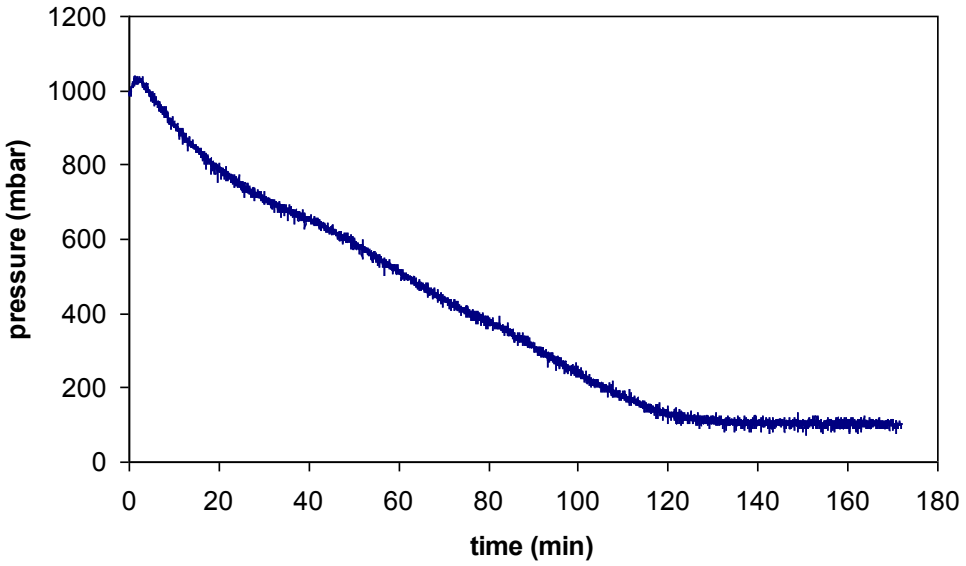

Fig 3.4 Typical pressure trend of the graphitisation reaction.

3.1.1 Accuracy tests performed using the new graphitization line

In order to test the new graphitization line, several samples were prepared and measured, in particular blanks and standard reference materials with certified ^{14}C concentration, i.e.:

[8] The dry pumping system is based on a diaphragm pump and a turbo molecular pump; the choice of these dry pumps was done in order to reduce possible contamination effects due to the presence of oil (for example the oil of a diffusion preliminary pumps).

- IAEA C7 (certified radiocarbon concentration 49.53±0.12 pMC), an Oxalic Acid standard reference material supplied by the International Atomic Energy Agency;
- VIRI D (certified radiocarbon age 2836±4 years BP): seeds from an archaeological excavation in Israel, dispatched to the laboratory within the Fifth International Radiocarbon Intercomparison (VIRI) campaign [Sco2007];
- VIRI S (certified radiocarbon concentration 109.96±0.04 pMC): barley mashes collected in a Scottish whiskey factory, dispatched to the laboratory within the Fifth International Radiocarbon Intercomparison (VIRI) campaign [Sco2010].

In Figures 3.5-8 the measured radiocarbon concentrations or radiocarbon age of these materials are reported.

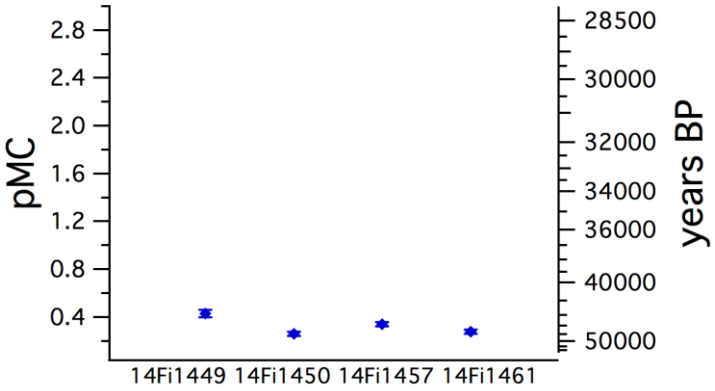

Fig. 3.5 Radiocarbon concentrations measured in blank samples expressed in percent of Modern Carbon; on the right y axis, the corresponding radiocarbon ages in years BP are also reported.

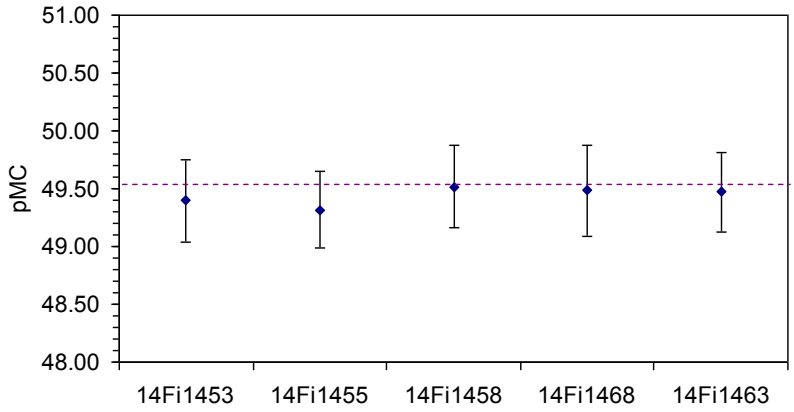

Fig. 3.6 Radiocarbon concentrations expressed in percent of Modern Carbon measured in standard IAEA C7 samples. The certified value (49.53±0.12 pMC) is represented with the dotted line. The experimental uncertainty on each sample concentration is quoted as 1 sigma.

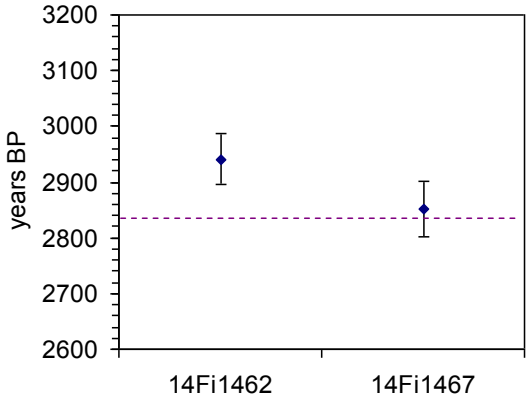

Fig. 3.7 Conventional radiocarbon ages expressed in years Before Present measured in VIRI D samples. The certified value (2836±4 years BP) is represented with the dotted line. The experimental uncertainty on each sample age is quoted as 1 sigma.

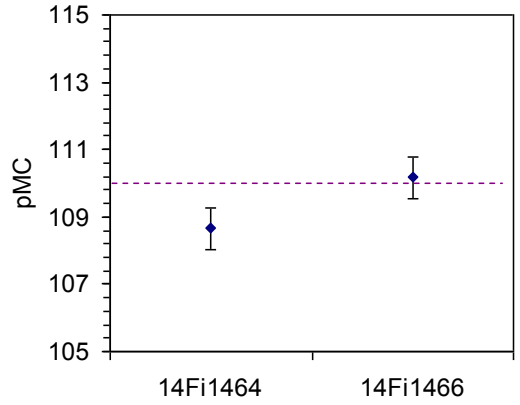

Fig. 3.8 Radiocarbon concentrations expressed in percent of Modern Carbon measured in VIRI S samples. The certified value (109.96±0.04 pMC) is represented with the dotted line. The experimental uncertainty on each sample concentration is quoted as 1 sigma.

The radiocarbon concentrations measured in blank samples are satisfactory and of the same order of magnitude of the typical concentrations measured in the first years of operation of the AMS facility at LABEC.

Concerning the standard materials, the data are consistent with the certified values. Only the ^{14}C concentration measured in samples 14Fi1462 and 14Fi1464 is slightly different with respect to the certified value; however, the two results are within 2 sigma confidence levels and thus can be accepted.

3.2 Upgrade of the AMS beam line

In chapter 2, the AMS beam line installed at the Tandem accelerator of LABEC was described; in particular, the rare isotope detection system based on the employment of an ionization chamber was presented.

Despite all the filters present on the AMS beam line and as a consequence of recombination or charge-exchange processes, some particles that simulate the same combination of energy, mass and charge of ^{14}C atoms might arrive on the detector. Considering the low energy resolution of the ionization chamber (about 70 keV) [Laz2007], identifying the residual atomic/molecular interferences with this system is not possible.

In the framework of an experiment funded by INFN (Istituto Nazionale di Fisica Nucleare), the final part of the AMS beam line has completely been re-designed: new detection system have been installed in order to improve the capability of discrimination, thus paving the way also to the measurements of rare isotopes other than ^{14}C. The upgrade has affected the line at the exit of the high energy electrostatic analyzer. The new channel is equipped with:

- a new silicon particle detector;
- a multiwire proportional chamber used as a beam profile monitor (BPM) for very low intensity ion beams (few tens of counts per second) [Tac2010];
- a time of flight system (TOF) with start and stop signals provided by modules based on micro-channel plates.

In Figure 3.9, a schematic drawing of the new channel is shown.

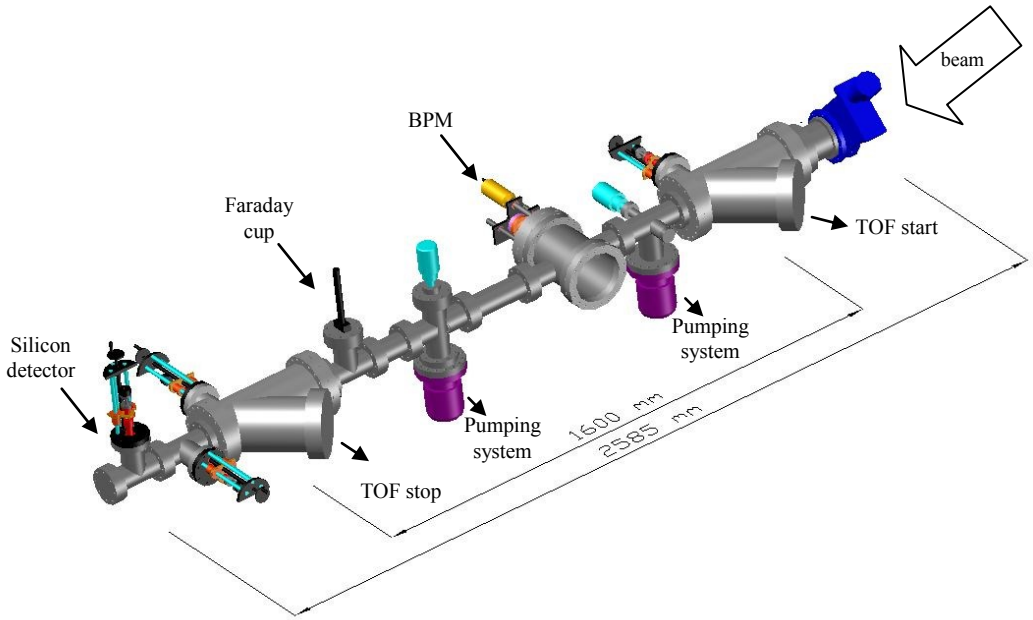

Fig. 3.9 Schematic drawing of the new AMS beam line installed at the exit of the electrostatic analyzer on the high energy side.

As a consequence of the addition of new elements, the AMS beam line was extended; in particular the rare isotope detector, now the silicon one, has been moved ahead of about 200 cm. In principle, this might have introduced some difficulties in the beam transport, since the only focusing element is represented by the electrostatic quadrupole doublets already installed at the exit of the electrostatic analyser, just before the new valve (see the blue valve in Figure 3.9).

In this section, only the upgrade concerning the new installed detector is described, being a part of this PhD work. The new detector is a Hamamatsu Silicon PIN photodiode S3590-09, having an active area of 100 mm^2 and a thickness of 300 μm. In Figure 3.10, the silicon detector and the retractable arm on which it is mounted are shown.

Fig 3.10 The new silicon detector (indicated by the black arrow) mounted on a retractable arm.

In Figure 3.11 a comparison between a spectrum acquired with the "old" ionization chamber and the new silicon detector is reported.

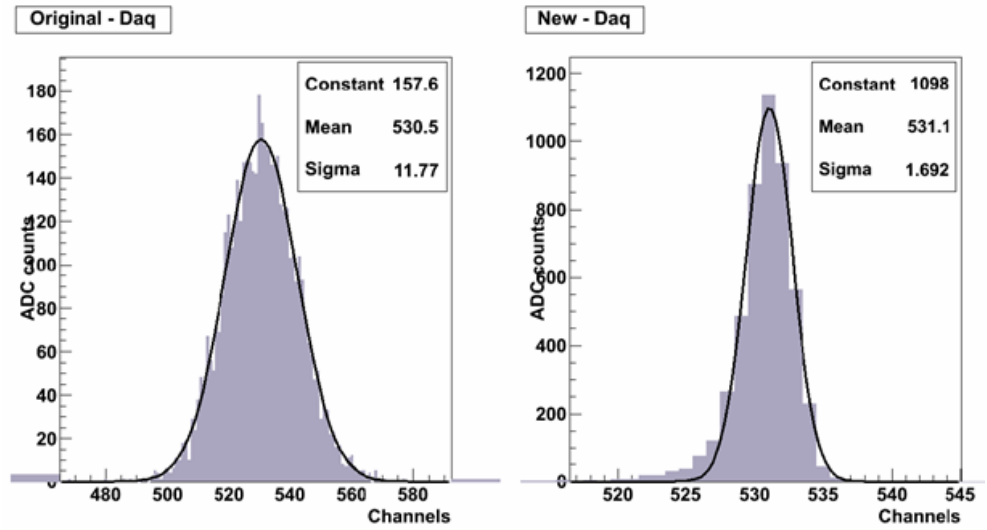

Fig 3.11 Beam energy spectra acquired with the ionization chamber and the silicon detector.

The comparison between the two detectors shows a remarkable improvement of the energy resolution by using the silicon photodiode. This means that it would be possible to identify the presence of possible particles having a slightly different energy with respect to the atoms of interest.

It's worth to notice that the use of this kind of solid state detector is possible thanks to the

low counting rate (see paragraph 2.7); however, it is well known that the exposure of this detectors to charged particle causes a significant deterioration in their performance. Serious changes of the energy resolution typically take place after the detector has been irradiated with about 10^8 ions/cm^2 [Kno1979]. To estimate the degree of deterioration of the new installed detector after two years of operation, we can do a simple calculation considering that, since its installation at the beginning of 2010, approximately 600 samples have been measured. Assuming for each modern sample:

- a counting rate of about 15 counts/s·cm^2;
- a measuring time of 60 min (which is needed to acquire a reasonable number of total counts to reach the desired level of precision);

it is possible to calculate a total flux of ~$3 \cdot 10^7$ ions/cm^2, still below the certified critical limit. It is worth to remember that this estimate represents an upper limit because most of the measured samples are characterized by a lower counting rate with respect to the modern samples (as one could expect, the oldest is the sample, the lower is the counting rate).

3.2.1 Accuracy tests of the upgraded AMS beam line

The upgraded AMS beam line was tested measuring the radiocarbon concentration in standard materials of certified ^{14}C abundance. The analyzed standard materials were IAEA C7, VIRI D, VIRI S (see paragraph 3.1.1) and:

- VIRI O (certified radiocarbon concentration 98.46±0.04 pMC), cellulose collected from Cambridge corresponding to 60 rings from a plateau period, dispatched to the laboratory within the Fifth International Radiocarbon Intercomparison (VIRI) campaign [Sco2010].

In Figures 3.12-16, the results of these test measurements are reported.

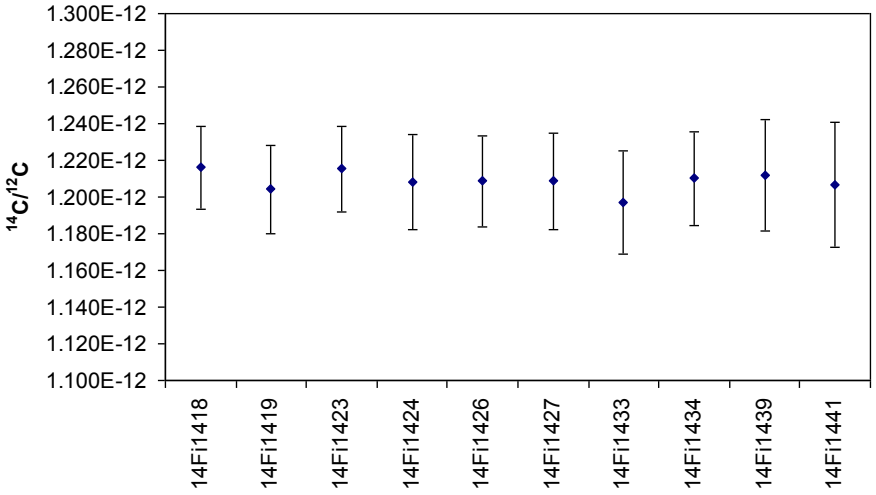

Fig 3.12 $^{14}C/^{12}C$ isotopic ratios measured in Oxalic Acid II standard material.

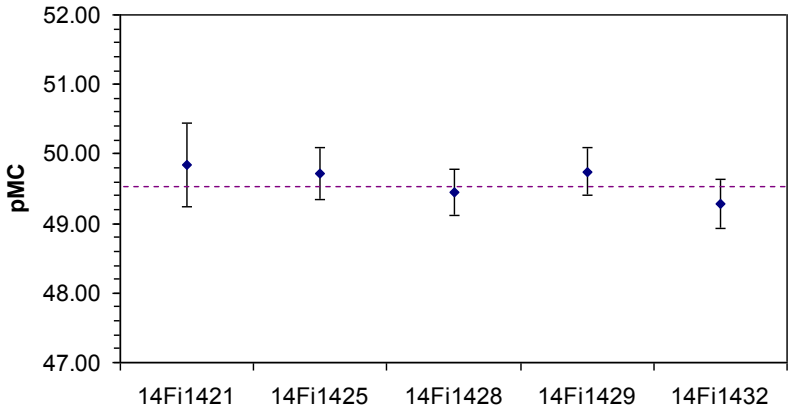

Fig 3.13 Radiocarbon concentrations expressed in pMC measured in IAEA C7 samples. The reference value (49.53±0.12 pMC) is represented by the dotted line. The experimental uncertainty on the measured concentrations is reported as 1 sigma.

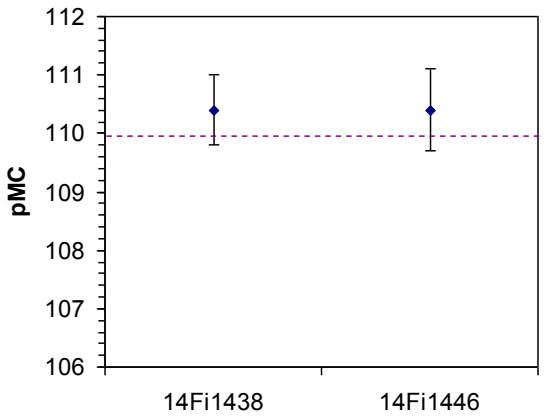

Fig 3.14 Radiocarbon concentrations expressed in percent of Modern Carbon measured in VIRI S samples. The certified value (109.96±0.04 pMC) is represented with the dotted line. The experimental uncertainty on each sample concentration is quoted as 1 sigma.

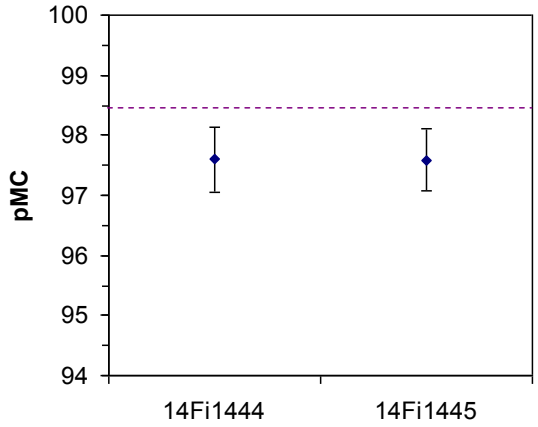

Fig 3.15 Radiocarbon concentrations expressed in percent of Modern Carbon measured in VIRI O samples. The certified value (98.46±0.04 pMC) is represented with the dotted line. The experimental uncertainty on each sample concentration is quoted as 1 sigma.

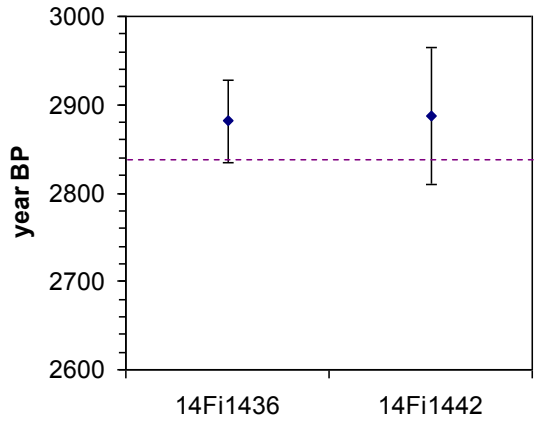

Fig 3.16 Conventional radiocarbon ages expressed in years Before Present measured in VIRI D samples. The certified value (2836±4 years BP) is represented with the dotted line. The experimental uncertainty on each sample age is quoted as 1 sigma.

As we can notice in Figure 3.12, the $^{14}C/^{12}C$ isotopic ratios measured in the modern standard samples are all consistent, demonstrating a good reproducibility of the measurement. The radiocarbon concentrations measured in the other reference materials are in a good agreement with the certified values, showing that the measurements are performed with high accuracy level. Concerning the VIRI O standards, the radiocarbon concentrations are slightly different with respect to the certified value; however, they are within 2 sigma confidence levels and thus can be accepted.

All things considered, the measurements shown above have been in agreement with the certified values, giving us the possibility to verify that the upgrade of the beam line have not

affected the beam transport.

3.3 New pre-treatment protocols

As it is explained in chapter 2, one of the most important steps of radiocarbon dating is the cleaning of the sample in order to remove all the contaminations.

The ABA standard protocol (described in paragraph 2.1.2) may not be sufficient to remove all possible contaminants present in the samples to be dated. For example, in particular preserving conditions of temperature and humidity, samples based on cellulose may have been more subjected to deterioration; these deteriorated parts may also be the more contaminated, thus we need a specific procedure to remove them extracting only a chemical sub-fraction that has remained stable during the time. In addition, when dating restored items, there can be the need to use particular organic solvents to remove the products applied in the restoration (in fact, being usually these products of synthetic origin, they can introduce a fossil contamination). In the next paragraphs, two new chemical protocols tested on wood and paper samples are presented.

3.3.1 Alpha cellulose extraction

Wood is a very common material used as support for artworks of all the centuries. In case of wooden samples, the better pre-treatment protocol has for example to be chosen according to the state of preservation. In addition, the identification of the wooden species can add further indications, as it can be inferred from the discussion below.

Wood is a material characterized by a complex structure. The principal wooden constituents are cellulose (including holo-cellulose, hemi-cellulose and alpha cellulose), lignin and resins. Cellulose is the most abundant wooden component and it is the organic fraction more subjected to deterioration, especially in extreme conditions of temperature and humidity. Lignin and resins are present in a lower percentage and are more stable than the celluloses; however, they can be also deposited after each tree ring has stopped the exchanges with the external environment and might be translocated over the different rings and thus over the different years. Hence, lignin and resins may contain a radiocarbon concentration that is not characteristic of one specific year. In some applications, in particular in reconstructing the

paleoenviromental conditions, this effect has been observed and studied [Paw2000, Paz2005, Rin2005].

The ABA standard protocol already leads to the suppression of lignin and resins. Anyway, in the case of samples collected from a wooden species that is very rich in those components, a more aggressive pre-treatment protocol can be better. Moreover, among the cellulose components, the isolation of a fraction that has remained stable over the time may be preferred; this fraction is the alpha cellulose. By definition, alpha cellulose is the component of a cellulosic material that is insoluble in a 17.5% solution of NaOH at 20°C [Anc2008].

In the literature, several well tested methods to isolate alpha cellulose in wood are reported; we have decided to use the protocol mentioned in [Paz2005], applying some modifications. In Figure 3.17, our protocol is summarized in a block diagram.

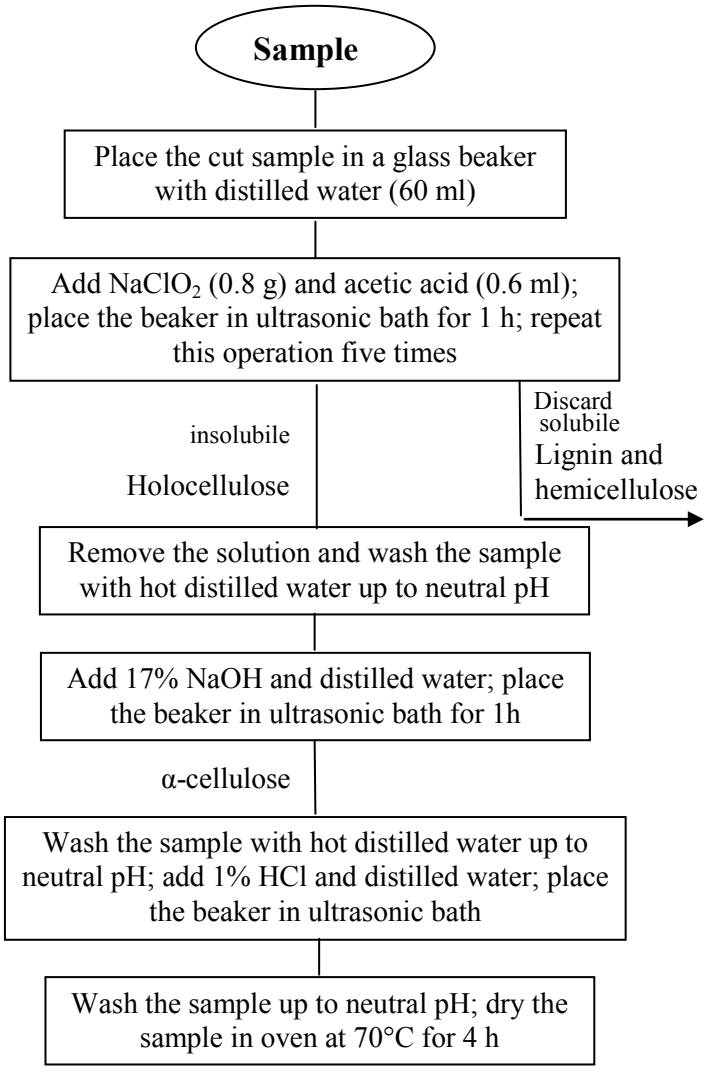

Fig 3.17 Block diagram of the alpha cellulose protocol set up for this work.

After this procedure, a mass loss of the order of 40-60% can be experienced for all treated samples.

We tested the new alpha-cellulose extraction protocol on wood and paper, which is a cellulose-based material; both materials are characteristics of the contemporary art samples that will be discussed in the next chapter. We measured:

- wood samples collected from oak timbers constituting the ceiling of a Sicilian church dated back to Renaissance;
- paper samples cut from Italian newspapers published during the 20th century (see paragraph 4.2 for the discussion about the relevance of such samples in Contemporary art).

To test the effectiveness of the new protocol, the same samples were pre-treated according to both this procedure and the more common ABA protocol. In Table 3.1, the results are summarized.

Material	**Sample**	**ABA protocol** ^{14}C *conc. pMC*	**alpha cellulose** ^{14}C *conc. pMC*
wood	Ivalsa 1	96.43 ± 0.38	95.80 ± 0.57
	Ivalsa 2	96.20 ± 0.33	95.77 ± 0.33
	Ivalsa 3	95.04 ± 0.27	95.74 ± 0.30
paper	COR38	97.94 ± 0.31	98.11 ± 0.31
	RES60	98.93 ± 0.38	98.37 ± 0.45
	CORS70M	111.59 ± 0.49	109.20 ± 0.41
	COR80	133.01 ± 0.36	132.96 ± 0.39
	COR83	123.45 ± 0.53	122.87 ± 0.44

Table 3.1 Radiocarbon concentrations (expressed in pMC) measured in wood and in newspapers samples: comparison of ABA protocol and alpha cellulose extraction. The experimental uncertainty is reported as 1 sigma.

As we can note, the radiocarbon concentrations relative to the two different pre-treatments are generally consistent between them. This result can be probably due to the fact that the measured samples were in a good state of preservation. As a consequence, we have decided to use the ABA protocol as the standard pre-treatment procedure for all similar samples that will be reported in the chapter 4.

3.3.2 The use of chloroform for contaminated samples

With the term restoration, all the operations necessary to preserve an historical-artistic object from the deterioration due to natural ageing, to particular conditions of temperature and humidity and to the action of biological agents are meant. Nowadays, these operations are usually performed using synthetic resins that are obtained by industrial-chemical reactions; the choice of these products with respect to natural remedies is due to a better stability over time (e.g. a minor yellowing and a major resistance to biological attacks). The synthetic resins are principally hydrocarbons-based, i.e. they are extracted from fossil oil and from its by-products. Being hydrocarbons characterized by a very low ^{14}C concentration that is well below the sensitivity of the AMS method, their not complete removal causes an apparent ageing of the sample (see the discussion in paragraph 2.1.1). In order to decide the better pre-treatment to apply to remove all the external substances, an exhaustive knowledge of the story of the sample and of its restoration stages can be thus recommended. Generally, the ABA standard protocol is not sufficient to remove this kind of contaminations; in addition, a most traditional mechanical cleaning with different tools or devices and the innovative laser ablation can appear too much invasive for the samples [Lop2011]. A complete removal is allowed using organic solvents, in particular petroleum solvents and chlorine-based products [Hor2010]. To be used in a radiocarbon measurement, these solvents must be characterized by a rapid evaporation; this is an important prerequisite in order to exclude contamination effects. In the literature, the most widely used protocol for radiocarbon applications is based on the Soxhlet extraction system [Bru2001], where the samples are treated with several organic solvents (each solvent is able to remove the traces of the previous agent in order to avoid any contamination effects). Therefore, this protocol is very time consuming.

Here, a new chemical procedure, which is easily operated, is presented. The new protocol is based on the use of chloroform ($CHCl_3$) as solvent.

This procedure was initially tested on two wood samples of known age treated with an acrylic resin usually applied for the consolidation of artistic supports. A sample was taken from an oak trunk; the piece was cut from the rings of the pre bomb period. The other sample was collected from a poplar trunk, taking care to get just the most external ring corresponding to 2009. The applied acrylic resin was Paraloid B72® [Roh2011], a copolymer of EMA/MA (ethyl methacrylate/methyl acrylate), dissolved in ethyl acetate solution. Before the application of the resin, small fragments of both wood samples were collected in order to

measure the “original” radiocarbon concentration (see the Wood_ABA column in Table 3.2) and so verify the possible apparent ageing due to the applied resin, and eventually the effectiveness of the pre-treatment procedures. These samples were treated using the ABA protocol.

In Figure 3.18, the two wood samples during the application of Paraloid are reported.

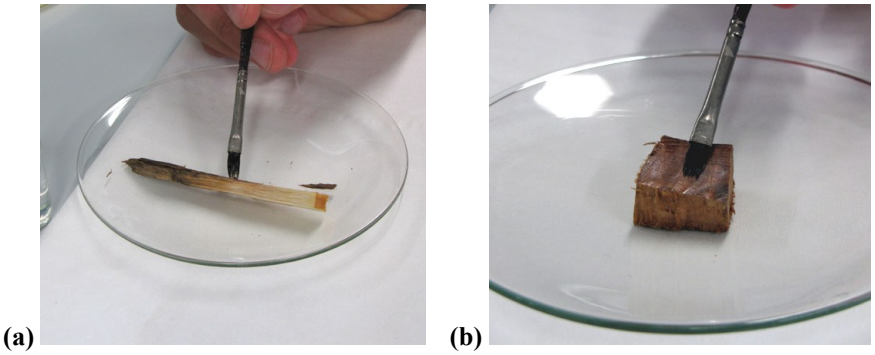

Fig 3.18 Picture of the poplar (a) and the oak (b) samples; the solution of Paraloid B72 and ethyl acetate was applied with a brush on all sides of the wooden fragments.

After the application of the resin, the samples were left for about one month in the laboratory in order to reproduce a natural ageing of the polymer; in fact, the temperature, humidity and irradiation conditions were not constant.

Afterwards, each sample was divided into two parts, each of them cut in little pieces. One part was directly treated using the ABA protocol (see the Para_ABA column in Table 3.2); the other (m ~ 20 mg) was put in a quartz tube, where 10 ml of chloroform were added; the tubes were placed on a magnetic agitator (see Figure 3.19).

Fig 3.19 Picture of the oak sample during the bath in chloroform on the magnetic agitator.

Samples had been soaked in chloroform for two days; during this period, the chloroform was periodically changed in order to permit a better reaction between the samples and the solution. Finally, the samples were removed from the solution and dried in fume hood at room temperature for two days at least. The mass loss after this procedure was about 50%. Finally, the wood samples were treated with the ABA protocol too (see the Para_Chl_ABA column in Table 3.2).

In Table 3.2, the radiocarbon concentrations measured in all the different treated samples are presented.

Sample	**Wood_ABA** ^{14}C *conc. (pMC)*	**Para_ABA** ^{14}C *conc. (pMC)*	**Para_Chl_ ABA** ^{14}C *conc. (pMC)*
Oak	97.42 ± 0.33	88.94 ± 0.78	97.66 ± 0.47
Poplar	104.31 ± 0.45	81.32 ± 2.06	104.21 ± 0.42

Table 3.2 Radiocarbon concentrations (expressed in pMC) measured in wood samples: comparison of the different used pre-treatment. Each result is the weighted average of two cathodes measured for each kind of wood samples, except in the case of the poplar sample "Para_ABA" (in this case, a simple average was performed since the two cathodes were not consistent, probably because of a non homogeneous application of Paraloid). The experimental uncertainty is reported as 1 sigma.

As we can notice, the two wood samples "Para_ABA" show a ^{14}C concentration lower than the measured concentration in the original samples; this effect corresponds to an apparent ageing. This result is the proof that Paraloid is source of contamination of dead carbon and that the ABA protocol is not sufficient to remove the acrylic resin. On the contrary, the radiocarbon concentrations measured in wood samples treated with chloroform ("Para_Chl_ABA") are consistent with the original samples, confirming the effectiveness of the new pre-treatment. This also means that chloroform, which is obtained from hydrocarbons, is completely evaporated and thus it itself does not represent a source of contamination.

A further check of the new pre-treatment protocol was performed measuring the adsorption of the characteristic bonds of the organic molecules in the infrared region by FTIR (*Fourier Transform Infrared Spectroscopy*); in fact, in this way, we can verify the presence of the synthetic resin.

As an example, only the FTIR spectra of the oak samples are reported. In Figure 3.20, the two spectra relative to the original wood sample (blue line) and to the sample after the

application of the acrylic resin (pink line) are shown. The bands of interest are at 1740 cm^{-1}, corresponding to the C=O stretching of ester bond, and at 750 cm^{-1}, corresponding to the C-Cl bond of chloroform. In particular, the ester bond is characteristic both of the acrylic resin and of the hemi-cellulose of the wood. Actually, as we can notice in the Figure 3.20, the intensity of the band at 1740 cm^{-1} is bigger in the case of the sample on which Paraloid was applied.

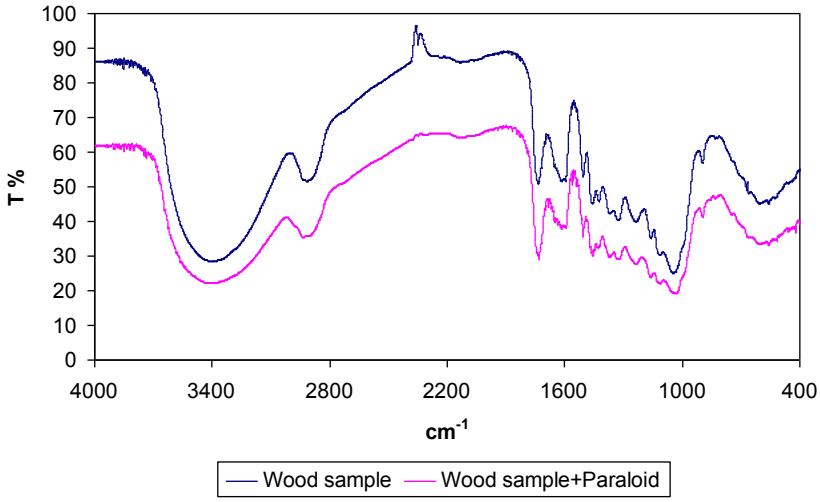

Fig 3.20 FTIR spectra of the oak samples: in blue the FTIR spectrum of the sample before all the treatments; in pink the FTIR spectrum of the sample after the application of Paraloid.

In Figure 3.21, a comparison between the spectra of the wood samples treated with the ABA (orange line) and with the chloroform based protocol (green line) is presented.

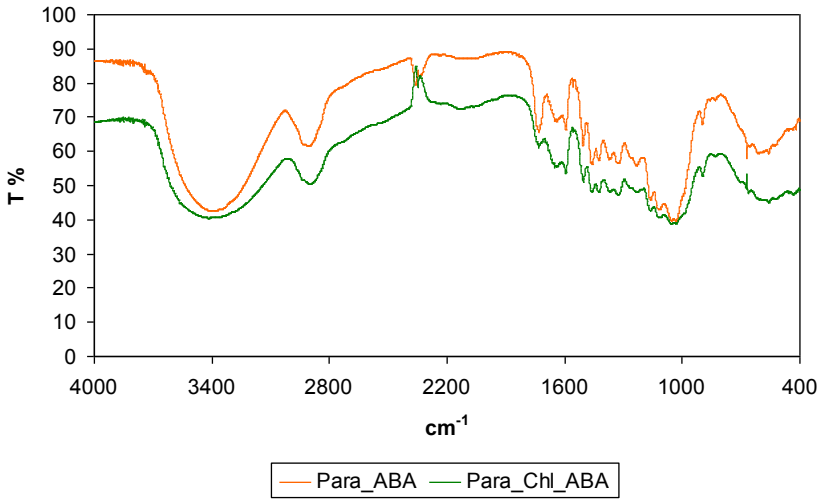

Fig 3.21 FTIR spectra of the Paraloid-treated oak samples: in orange the FTIR spectrum of the sample after the ABA protocol; in green the FTIR spectrum of the sample after the chloroform-based protocol.

We can observe that in the orange spectrum the peak at 1740 cm^{-1} corresponding to Paraloid is still present, displaying that the ABA standard protocol is not sufficient to remove the resin; this result is in agreement with the radiocarbon dating (see the Para_ABA column in Table 3.2). It can be noticed that the band is less intense than in the pink spectrum in Figure 3.20, but this is due to the effect of the ABA treatment on cellulose. Indeed, during the bath in NaOH and as a consequence of the heating during the acid steps [YOh2005], the hemi-cellulose ester bonds are partially broken and so dissolved in the solutions. On the contrary, in the green spectrum the bands corresponding to Paraloid and to the C-Cl bond (~750 cm^{-1}) are not visible, supporting the radiocarbon dating (see the Para_Chl_ABA column in Table 3.2) and proving the effectiveness of the new chemical pre-treatment.

Chapter 4
Radiocarbon measurements on samples of the 20th century

As already mentioned in chapter 1, radiocarbon dating can be a very powerful method to also investigate the recent past. Among all the several forensic applications, the identification of fakes of contemporary artworks has been mentioned. Since this PhD work has been focused on verifying the advantages and the limits of radiocarbon for the identification of forgeries of artworks of the last century, in this chapter the radiocarbon measurements performed on different materials typically used in art are presented.

4.1 The "local" bomb peak curve

In paragraph 1.3.2, the causes of the huge increase of the radiocarbon concentration in atmosphere during the second half of the 20th century were explained. Furthermore, the four calibration curves found in the literature that reproduce the distribution of the ^{14}C concentration as a function of the latitude were presented. Since some regional or local effects may however occur, causing a not uniform distribution of the radiocarbon concentration on earth [Kaw2007, McG2004, Qua2005, Rak2010], as a preliminary work, we measured a "local" bomb peak curve. We chose a non-industrial site in central Italy, Mount Amiata (42°N, 11°E) in Tuscany, and we measured the radiocarbon concentrations in tree rings collected from an oak which was cut in 2008 when the tree was about eighty years old (see Figure 4.1).

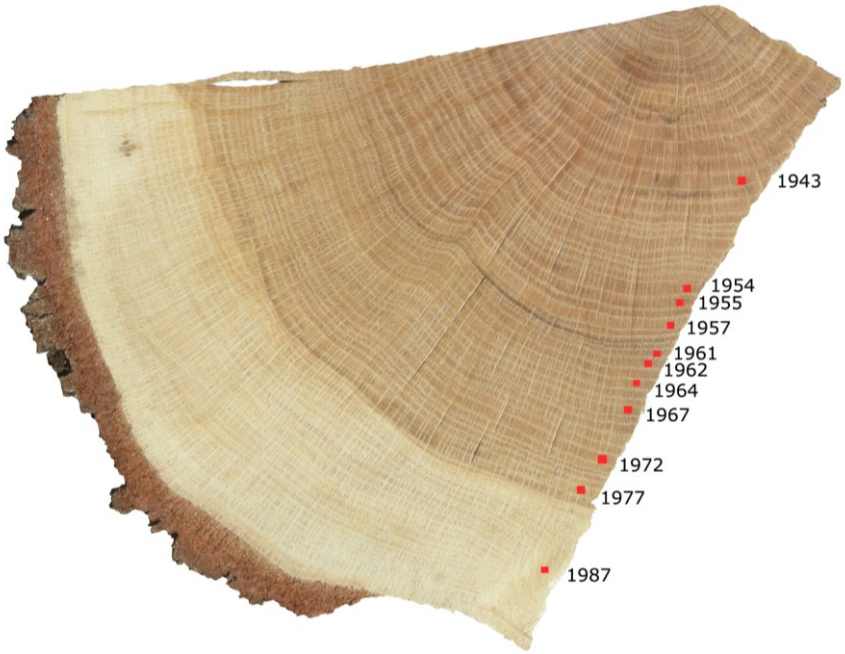

Fig 4.1 Picture of the oak trunk: tree rings are well visible. The tree rings from which the measured samples were collected are indicated with red spots, together with the corresponding years.

All collected wooden samples were treated by the ABA protocol. In Table 4.1 the samples, the corresponding years and the measured radiocarbon concentrations are reported.

Sample name	year	^{14}C conc. (pMC)
AMIATA43	1943	97.91 ± 0.40
AMIATA54	1954	98.61 ± 0.67
AMIATA55	1955	100.89 ± 0.76
AMIATA57	1957	106.19 ± 0.41
AMIATA61	1961	124.08 ± 0.42
AMIATA62	1962	123.98 ± 0.63
AMIATA64	1964	182.01± 0.54
AMIATA67	1967	167.88 ± 0.57
AMIATA72	1972	152.19 ± 0.45
AMIATA77	1977	134.46 ± 0.40
AMIATA87	1987	117.03 ± 0.52

Table 4.1 Samples collected from the oak trunk, showing the year of growth and the measured radiocarbon concentrations (expressed in pMC).

Our experimental results can be compared to the reference curve Bomb04NH1 (see paragraph 1.3.2), which describes the ^{14}C concentration in atmosphere in the area from the North Pole to the ~40°N latitude. As we can notice in Figure 4.2, the measured samples are in a good agreement with the atmospheric data reported in the literature. This means that, if some local effects are present, they are not so significant to be measured.

As a consequence, we have decided to use the Bomb04NH1 curve as the reference curve to calibrate all the measured radiocarbon concentrations of the samples that will be presented in the next paragraphs.

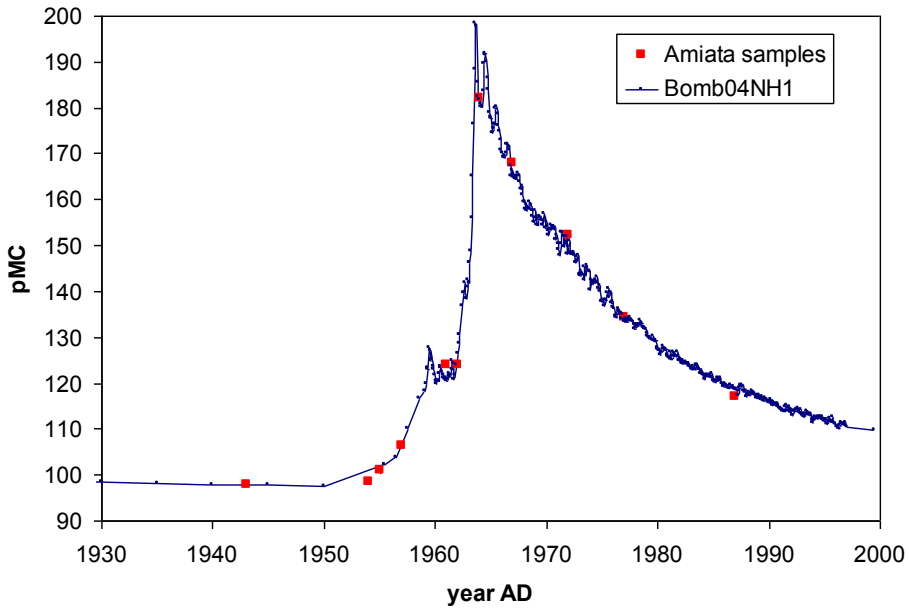

Fig 4.2 Comparison between the Bomb04NH1 curve and the experimental data obtained from the tree rings samples. In the used scale for the y-axis, the experimental error bars are not visible.

4.2 Measurements on paper samples

As far as paper is concerned, two different kinds of samples were analysed: newspapers and fine paper samples. Of course, newspapers were chosen not for their artistic value but because they might represent "dated" items, if we consider that we might correlate them to the date printed on the published issue. With regard to fine paper, the samples were collected from cotton cardboard paper used for limited edition prints.

4.2.1 Newspaper samples

28 samples were collected from Italian newspapers issued since 1938 until present. In agreement with the data reported in Table 2.1, the masses were of the order of 20 mg (corresponding to an area of about 1 cm^2).

As a preliminary investigation, in order to give a more comprehensive interpretation of the measurement results, the composition of the raw material was analyzed. In fact, paper can be in principle produced either from trees or from annual plants. According to the literature [Jer2010, Wei1997], low quality paper, as the paper for dailies is supposed to be, is usually made of chemi-mechanical pulp from wood. To verify this, the collected paper samples were analysed by SEM (*Scanning Electron Microscopy*). As an example, Figure 4.3 shows a fragment of a scanned newspaper sample (sample "COR66"). SEM image confirms the use of wood: indeed, the typical fibres of wood and the pits of the wooden membranes and tracheids are easily recognizable (see the pits indicated with a red arrow in the Figure 4.3). The flat shape of the fibres is due to the manufacturing processes.

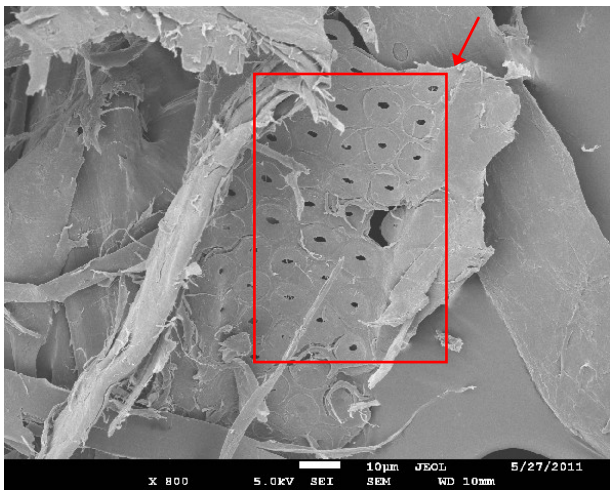

Fig 4.3 SEM image of a fragment from sample "COR66": the black holes (indicated with a red arrow) are the characteristic pits of the wooden membranes and tracheids.

All the samples were subjected to the ABA pre-treatment[9]. In Table 4.2, the ^{14}C concentrations measured in newspaper samples are presented.

[9] Actually, no significant differences in the measured ^{14}C concentrations had been shown between samples prepared according to the alpha cellulose extraction protocol and the standard ABA procedure (see paragraph 3.2.1).

Sample name	Year of publication	^{14}C conc. (pMC)
COR38	1938	97.94 ± 0.31
COR47	1947	97.06 ± 0.31
COR50A	1950	97.61 ± 0.30
COR50B	1950	97.11 ± 0.32
RES53	1953	97.05 ± 0.61
CDI58	1958	97.59 ± 0.35
RES60	1960	98.93 ± 0.38
STA63	1963	105.09 ± 0.36
COR66	1966	120.54 ± 0.29
COR67	1967	135.38 ± 0.57
COR68	1968	139.39 ± 0.41
COR69	1969	133.86 ± 0.37
CORS70M	1970	111.59 ± 0.49
CORS70S	1970	105.28 ± 0.46
RES76	1976	115.63 ± 0.39
COR78	1978	125.81 ± 0.41
COR79	1979	119.90 ± 0.33
COR80	1980	133.01 ± 0.36
CORSP80	1980	119.18 ± 0.33
COR81	1981	124.58 ± 0.39
COR83	1983	123.45 ± 0.53
COR84	1984	125.70 ± 0.34
COR85	1985	127.81 ± 0.35
COR91	1991	120.09 ± 0.47
COR93	1993	121.00 ± 0.51
REP96	1996	125.10 ± 0.53
COR98	1998	119.71 ± 0.40
COR09	2009	113.05 ± 0.46

Tab 4.2 Radiocarbon concentrations measured in newspaper samples; the experimental uncertainty is quoted as 1 sigma.

Our experimental data can be compared to the Bomb04NH1 curve (see Figure 4.4).

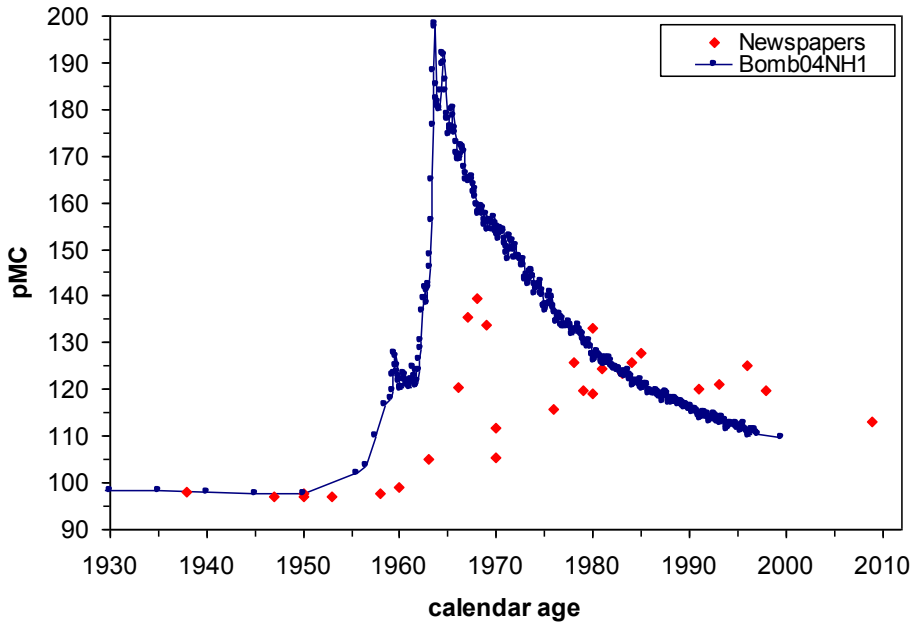

Fig 4.4 Radiocarbon concentrations measured in newspaper samples compared to the Bomb04NH1 curve. The newspaper samples are plotted versus the year of publication. The experimental error bars are not visible in the chosen scale.

Looking at the Figure 4.4, we can clearly notice that it is possible to discriminate newspaper samples that are produced before and after 1960.

However, some differences between the experimental results and the data reported in the literature are remarkable:

- the ^{14}C peak in paper samples is shifted towards more recent times with respect to the atmospheric values (this shift is about five years);
- the maximum concentration measured in paper samples is lower than the maximum value of Bomb04NH1.

With regards to these discrepancies, the experimental results are not surprising. As it can be inferred from the literature and as it has been confirmed by the SEM analyses, the newspapers raw material is wood. Thus, for each sample, what we measured is a sort of mean value of the ^{14}C concentrations of the rings forming the tree and that had been mixed together to produce that sheet of paper (considering that each ring contains a radiocarbon concentration that is characteristic of the year of its growth). In order to verify the possibility to analytically describe the experimental data, we tried to apply a very simple model. The radiocarbon concentration measured in each paper sample pMC_{calc} can be written as:

$$pMC_{calc} = \frac{1}{M_{sample}} \sum_{i=1}^{N} m_i \, pMC_i \qquad (4.1)$$

where M_{sample} is the mass of the whole paper sample, N is the number of the rings mixed in a single sheet, m_i is the mass of a single ring and pMC_i is the radiocarbon concentration of that single ring.

As a clear simplification, if we consider that each tree ring contributes for the same mass, i.e. $m_i=m_j$, we can write the model as:

$$pMC_{calc} = \frac{1}{N} \sum_{i=1}^{N} pMC_i \qquad (4.2)$$

Since a priori it is not possible to know the age of the tree from which the sample was obtained and thus the number N of the tree rings, three different reasonable cases were simulated, i.e. making an average on 20 years, 30 years and 20 years with an offset of 3 years. The models calculated from the equation 4.2 are compared with the experimental results in Figure 4.5.

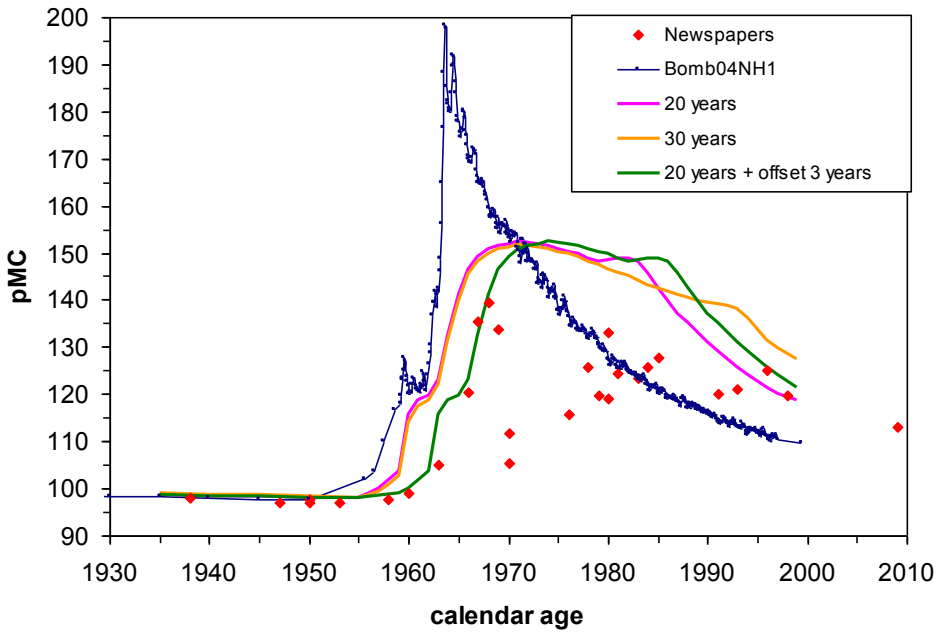

Fig 4.5 Comparison between the measured newspapers samples and the models based on the equation 4.2.

As we can notice in Figure 4.5, any calculated curve does not fit the experimental results. Only in the case of the trend indicated with the green line, i.e. using twenty as the total number of tree rings in each sample and adding a three years offset, there is a limited overlap with the measured radiocarbon concentrations. The chosen offset of three years can be reasonable supposing that some external rings were removed during the manufacturing processes and/or paper was not immediately used after its production. The remarkable discrepancy noticed for newspapers produced after about 1970 can be explained considering that the equation 4.2 describes a very simplified situation, not taking into account many variables. These variables especially concern the manufacturing processes; for examples, we do not know the exact ages of the trees used to obtain the sheet, how many rings were removed in the processes and when the custom of recycling paper was introduced. Since all these processes are typically hedged in professional secret by industries and are not well traceable, their description in a mathematical model is not so simple. As a consequence, we have to finally summarize that, even though we are able to perform radiocarbon measurements with a high precision (see the experimental uncertainties reported in Table 4.2), it is not possible to match each radiocarbon concentration to the corresponding calendar year in which the paper was produced.

4.2.2 Fine paper samples

The fine paper samples were collected from cardboard used as support of limited edition drawing prints. Each of the 9 samples, taken from the edges of the cardboards, was of the order of 40 mg[10], even though the sample dimensions were quite small (about 1 cm^2).

Measuring the radiocarbon concentration of this kind of samples can be interesting since the raw material used to manufacture the paper is different from the case of newspapers. Indeed, fine art papers are usually produced from cotton. To verify this, collected samples were also studied by SEM. Figure 4.6 shows a SEM image of a paper fragment (sample "Seve1965"); the analysis confirmed the use of cotton fibres: the cotton fibres are easily recognizable thanks to the spiral disposition of the fibrils around the principal fibre axis.

[10] These masses are justified by a higher specific weight of this kind of paper with respect to the common paper sheets.

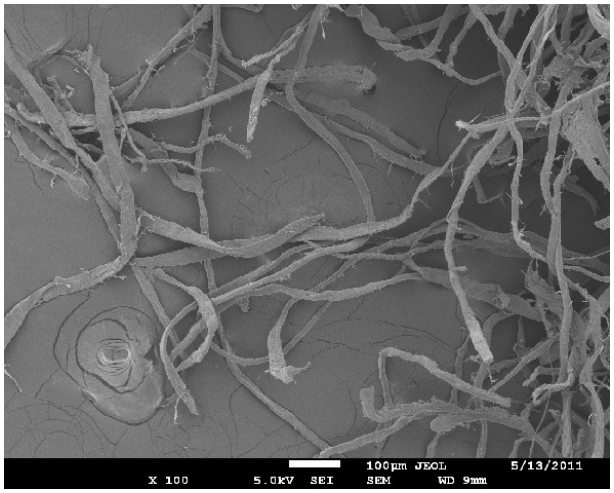

Fig 4.6 A SEM image of the samples "Seve1965": the characteristic twisted shape of cotton fibres is recognizable.

Unlike newspaper samples, since this kind of paper is obtained from cotton that is a short living plant, the measured radiocarbon concentrations in cardboards will be characteristic only of one year, corresponding to the year during which the plant lived.

Before the ^{14}C measurement, these samples were also treated following the ABA standard protocol.

The measured radiocarbon concentrations are reported in Table 4.3. We can observe that all the measured radiocarbon concentrations are bigger than 100 pMC, hence the samples were produced after 1950; the experimental results are so in agreement with the expected value.

Sample name	Printing year	^{14}C conc. (pMC)	Calibrated age(*) (AD)
Carma60	1960	102.80 ± 0.63	1954-1956
Abe61	1961	111.75 ± 0.79	1957-1958 1993-2000
Far63	1963	111.45 ± 0.68	1957 1993-1999
Seve65	1965	117.41 ± 0.82	1958-1959 1986-1990
Cobra68	1968	147.66 ± 0.80	1962-1963 1970-1973
Mac70	1970	101.60 ± 0.59	1953-1956
Moore71	1971	137.29 ± 0.98	1962 1974-1977
Candi76	1976	131.69 ± 0.36	1962 1977-1979
Papa80	1980	132.01 ± 0.63	1961-1962 1977-1979

(*) *Calibrated time intervals are quoted at 68% level of probability.*

Table 4.2 For each cardboard sample the printing year, the measured radiocarbon concentration and the corresponding calibrated age are reported.

To have an estimation of the real calendar age of the sample (see also Table 4.2), we can use one of the most common programs based on bayesian statistics, i.e. OxCal version 4.1 [Ram2009] or we can just intercept the bomb curve drawing a horizontal line centred on the measured radiocarbon concentration. In Figure 4.7, such an example of calibration (sample "Far63") is reported.

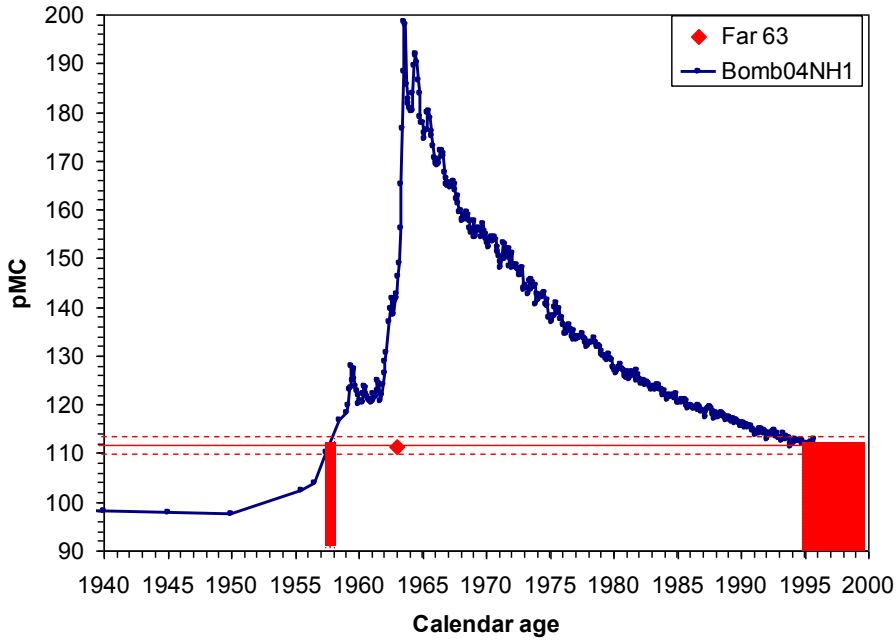

Fig 4.7 Example of calibration (sample "Far63") by intercepting the Bomb04NH1 curve with a horizontal line centred on the measured radiocarbon concentration. The measured radiocarbon concentration is also reported as a function of the printing year (see the red diamond). With red solid line the projection of the measured concentration is represented; the corresponding experimental uncertainty (1 sigma) is represented with red dotted line.

We can notice that the calibration curve is intercepted in two time intervals and that the two intervals spans are different. Concerning the two calibrated ages, it is obvious that we can exclude one of them if we have independent information. The fact that the two time intervals spans are different is a consequence of the characteristic trend of the curve. Indeed, for the period 1950-1965, the significant differences of ^{14}C in atmosphere between consecutive years allow us to date recent samples with a resolution of one or few years. After about 1965, since the slope of the calibration curve is lower, slightly larger time intervals can be obtained. Therefore, with respect to the "traditional" dating of the archaelogical samples for which only a great interval of calibrated age can be obtained, thanks to the characteristic behaviour of the calibration curve, we are able to date and calibrate samples of this period with very small uncertanties.

Comparing the calibrated time intervals with the year when the fine paper sample was printed, we can notice that there are some discrepancies. Generally, the first calibrated time interval is prior to the expected date. This years offset can be due to a reasonable time gap between the year when the plant was cut and when the cardboard was used.

4.3 Measurements on canvas samples

The radiocarbon measurements on canvas samples presented in this paragraph can be divided into two groups: canvas of the period 1900-1950 and canvas of the period after 1950.

The typical masses of the measured 11 canvas samples that were collected from the rear edges of paintings were of the order of 40 mg. These masses are not surprising; in fact, these samples were not completely clean. It is very common to find many overlapping layers on the canvas used as support of paintings, such as preparations, pigments and binders. These layers may be sources of possible carbon contamination and thus have to be completely removed before the AMS measurement. The removal of preparation layers with a scalpel can sometimes be very difficult, especially in the case of canvas of industrial manufacture, when these layers are very sticky to the fibres. To give an example about the difficulty to remove the industrial preparation layers, some pictures of the sample "Can1980" before and during the pre-treatment are shown in Figures 4.8 and 4.9. On the recto (Figure 4.8 a), it is possible to notice the industrial preparation layer, which is very thick and compact. The preparation layer has crossed the texture of the canvas (visible on the verso side in Figure 4.8 b). On the verso side, we can notice the brownish colour of the textile; since the original colour of the fibre (indicated with a red arrow) is almost white, we can suppose that this colour can be due both to the application of other products and to the dirt settled over the time.

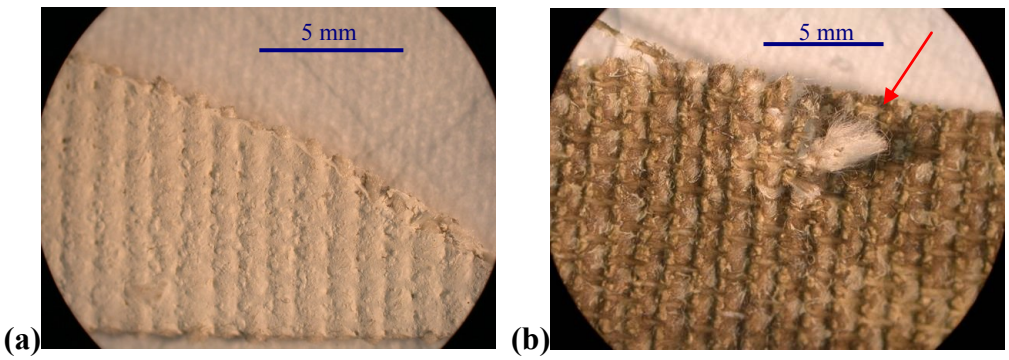

Fig 4.8 Sample "Can1980", recto (a) and verso (b). With the red arrow, a clean fibre is indicated: the different brownish colour of most of the fibres suggests that on the verso side some products had been also applied.

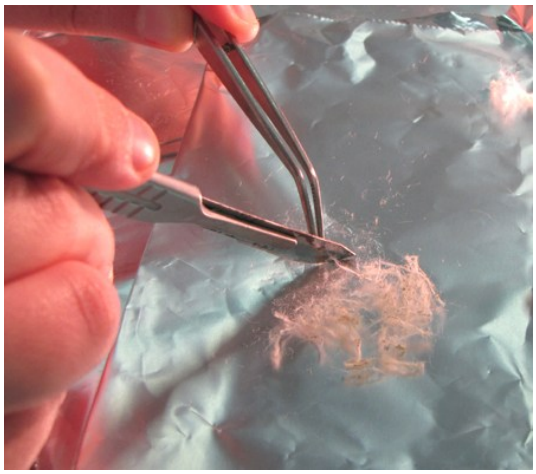

Fig 4.9 Sample "Can1980" during the physical pre-treatment: each single fibre is scratched with scalpel in order to completely remove the overlapping layers.

After the physical pre-treatment, all the samples were washed in ultrasonic bath in a solution of distilled water and acetone (1:1) in order to remove the presence of some organic contaminants (e.g. glue). Afterwards, the samples were dried in vacuum at 100°C over night to enhance (by degassing) the removal of some resinous traces [Rei1999]. Then, all the samples were treated using the ABA standard protocol.

4.3.1 Textile fibres in modern and contemporary art

After the above description of some characteristics of the canvas samples, in this paragraph, an overview about the origin of the textile fibres used for artworks is presented.

For centuries, the typical raw materials used to manufacture canvas for painting were only cotton, flax, hemp and jute. Since the end of the 19th century, a great number of new fibres have been produced. These new textiles are classified as artificial or synthetic depending on the raw material and the manufacturing processes. Even though their use in fine art applications is very limited, a brief description is necessary.

As a consequence of the industrial revolution, new industrial manufacturing processes and new fibres were developed in Europe and in the United States. The new textiles were produced treating the natural fibres, usually cotton, with chemical solvents (synthesized from hydrocarbons) in order to improve the physical properties of the single fibre. These fibres were called artificial; the most common, used also in contemporary artworks, were rayon, viscose and acetate. In these cases, the manufacturing processes, based on the use of

hydrocarbon-based solvents, introduce a variable fraction of dead carbon in the sample. This means that, measuring the radiocarbon concentration in the modified fibres, an apparent ageing of the sample is observed.

Another important development in the textile industry was the discovery of nylon in 1927. It was the first synthetic fibre and signed the beginning of the use of fibres produced just by chemical processes. Among all the chemical fibres, we can just mention polyesters, polyamides and vinyl compounds. The principal use of these textiles was especially in the military field or in the clothing industry. Since the synthetic fibres are obtained only by hydrocarbon-based solvents and being petroleum infinitely old for radiocarbon dating, these textiles cannot be dated.

In summary, only canvas samples obtained from natural fibres can be of course dated by radiocarbon; in the other cases, the dating is not possible. For this reason, to have a reliable radioarbon date, a preliminary analysis to identify the fibres is necessary. The identification of fibre type is not achieved thanks to a simple comparison of textures and colours of the textiles. As in the case of paper (see paragraph 4.2), the best approach recommends a careful analysis by electron microscope (SEM).

All the collected canvas samples were thus analyzed in order to verify that all fibres were of natural origin. For instance, three canvas samples ("Can1925", "Can1966B" and "Can1966N") are shown in Figures 4.10-12. The cotton fibres are easily recognizable thanks to the twisted shape (see Figure 4.11 b). The flax fibres are instead characterized by the so-called "elbows" i.e. rings similar to the tree rings. These elbows represent fragility points of the fibre and in fact, when the fibre is deteriorated, they are broken. In Figures 4.10 (b) and 4.12 (b) the flax fibres are well identifiable; the elbows are indicated with red arrows. In the first case ("Can1925"), the flax fibre is in a good preservation state, while in "Can1966N" the fibres are broken next to the elbows.

(a)

(b)

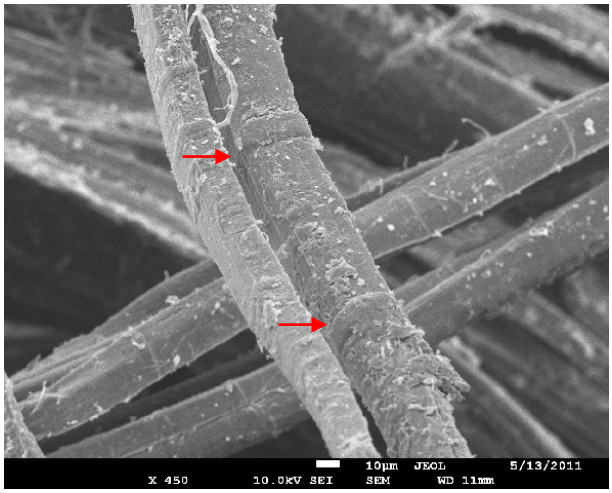

Fig 4.10 Sample "Can1925": picture of the sample under optical microscope (a) and picture by SEM (b). The flax fibres are well recognizable thanks to the characteristic elbows (shown with red arrows) of the single fibre.

(a)

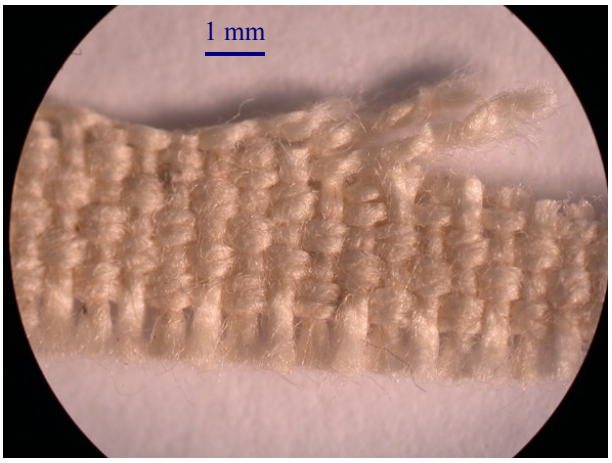

(b)

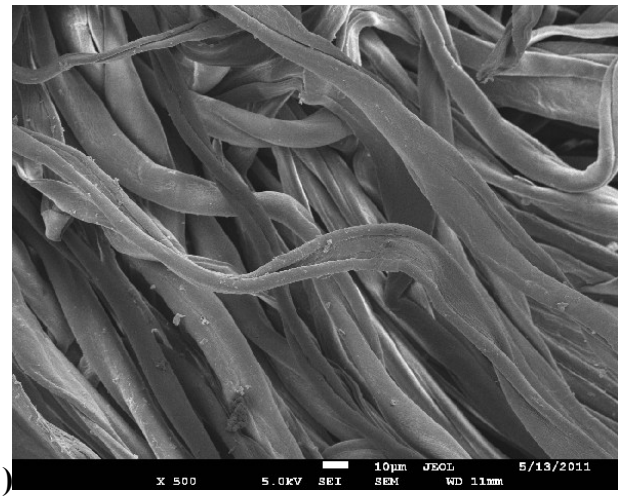

Fig 4.11 Sample "Can1966B": picture of the sample under optical microscope (a) and picture by SEM (b). This canvas was obtained from cotton plant; the characteristic shape of cotton fibres is well visible.

(a)

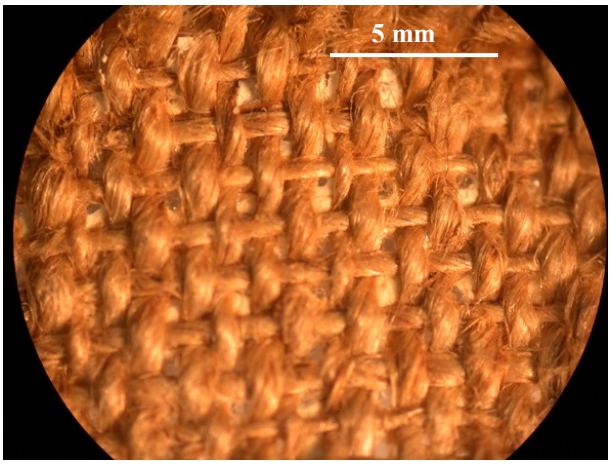

(b)

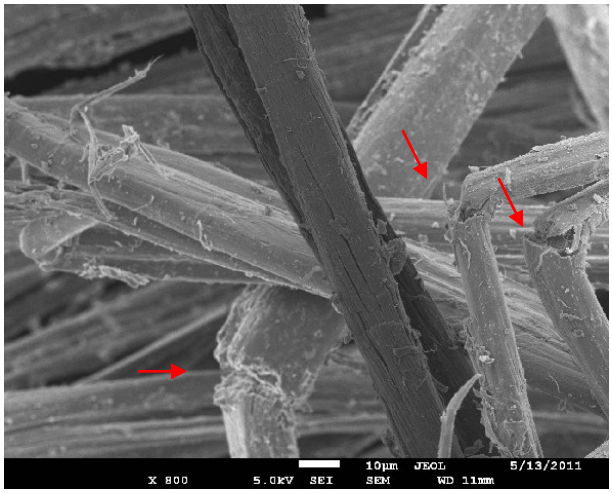

Fig 4.12 Sample "Can1966N": picture of the sample under optical microscope (a) and picture by SEM (b). The canvas is of natural origin: the flax fibres are identifiable thanks to the broken elbows (indicated with red arrow).

Summarizing, all the canvas samples to be dated scanned by SEM were obtained from natural fibres, either cotton or flax. As in the case of cotton cardboard papers, the canvas samples are so obtained from annual plants, hence the measured radiocarbon concentrations will be characteristic only of the years during which the plants lived. In the following, the radiocarbon measurements on these samples will be presented.

4.3.2 Canvas samples of the period 1900-1950

Concerning the canvas of the pre bomb period, 4 samples were measured. In Table 4.3 the measured radiocarbon concentrations are reported.

Sample code	Year on painting	^{14}C conc. (pMC)	Calibrated age (AD)
Can1910	1900-1910	97.77 ± 0.34	Modern
Can1922	1922	98.64 ± 0.30	Modern
Can1925	1925	99.17 ± 0.32	Modern
Can1928	1928	97.32 ± 0.48	Modern

Table 4.3 Data of canvas samples collected from paintings signed in the period before 1950: the year painted on the canvas, the measured radiocarbon concentrations and the corresponding calibrated age are reported.

As we can note in the column of calibrated ages, the canvas samples can be only defined as modern, without specifying any precise time interval, according to the common use of the international radiocarbon community. This is a consequence of the so-called Suess effect (see paragraph 1.3.2). In order to better understand this classification, an example of calibration (calculated for the sample "Can1925", nominally dated back to 1925) is shown in Figure 4.9. The calibration was performed using OxCal program, with reference to the IntCal09 calibration curve.

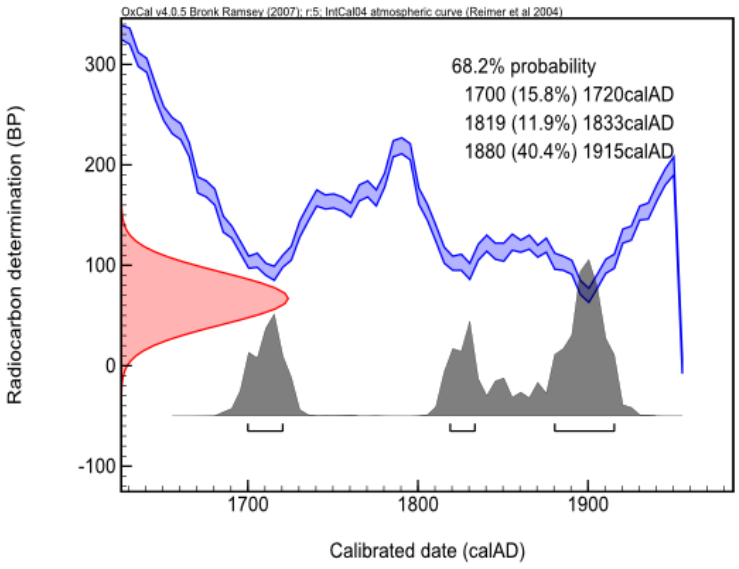

Fig 4.13 Calibration of the sample "Can1925": the calendar age is on the x axis; the measured radiocarbon age is represented on the y axis as a Gaussian distributed variable (in red); in blue, the calibration curve is drawn. The distribution of probability of the calibrated age is represented in grey; the calibrated time intervals quoted at a probability of 68% are also indicated.

In the graph reported in Figure 4.13, the calendar age is shown on the x axis, the measured radiocarbon age is represented on the y axis as a Gaussian distributed variable (in red); the

calibration curve is drawn in blue. The distribution of probability of the calibrated age is represented in grey; the calibrated time intervals corresponding to a level of probability of 68% are also indicated. The calibrated age of the sample "Can1925" corresponds to three separated probable time intervals, i.e 1700-1720, 1819-1833 and 1880-1915, considering a level of probability of 68%. If we consider a higher level of probability, these time ranges of course become larger: a period since 1810 to 1920 is even identified when we consider a level of probability of 95%. This is due to the quite horizontal trend of the calibration curve in the period between 1650 and 1950. Even though, in this particular case, a time interval in the second half of the 18^{th} century appears not to be included among the probable periods of the calibrated age, it is evident that the measurements of the ^{14}C concentration does not give us any useful information to discriminate whether this sample was of the 18^{th} century or the 19^{th} century or the first years of the 20^{th} century. Therefore, being not possible to solve the ambiguity among these most recent centuries, the sample is classified only as modern.

However, it's worth to be noticed that all the measured radiocarbon concentrations in the canvas samples are in agreement with the expected value.

4.3.3 Canvas samples of the bomb peak period

As far as paintings on canvas of the bomb peak period are concerned, 7 samples were collected. In Table 4.4 the experimental results and the calibrated ages are reported.

The radiocarbon measurements show the capability to discriminate samples of the Bomb Peak period from the samples prior to 1950.

Concerning the calibration, we can also notice that for most of the canvas samples more than one calibrated time intervals are obtained. As it is explained in paragraph 4.2.2, this is related to the characteristic trend of the bomb peak curve. It is obvious that we can just exclude one of the two calibrated time intervals if we have independent information about the dated object, e.g. historical documents.

Sample code	Year on painting	^{14}C conc (pMC)	Calibrated ages(*) (AD)
Can1962	1962	109.19 ± 0.76	1956-1957 1995-2000(**)
Can1965	1965	167.55 ± 2.18	1965-1966
Can1966B	1966	109.09 ± 0.38	1956-1957 1997-2000(**)
Can1966N	1966	171.1 ± 1.09	1965-1966
Can1971A	1971	172.98 ± 0.55	1965-1966
Can1971C	1971	121.83 ± 0.80	1959-1962 1982-1985
Can1980	1980	112.76 ± 0.64	1957-1958 1991-1995 1998-2000(**)

(*) *Calibrated time intervals are quoted at 68% level of probability.*

(**) *The upper limit of 2000 in the calibrated time interval is due to the fact that the Bomb04NH1 curve just covers the period until the mid 1999.*

Table 4.4 Data of canvas samples of the bomb peak period: the year painted on canvas, the measured radiocarbon concentrations and the corresponding calibrated age are reported.

An example of calibration, simply obtained by intercepting the Bomb04NH1 curve with the projection of the measured radiocarbon concentration, is presented in Figure 4.14.

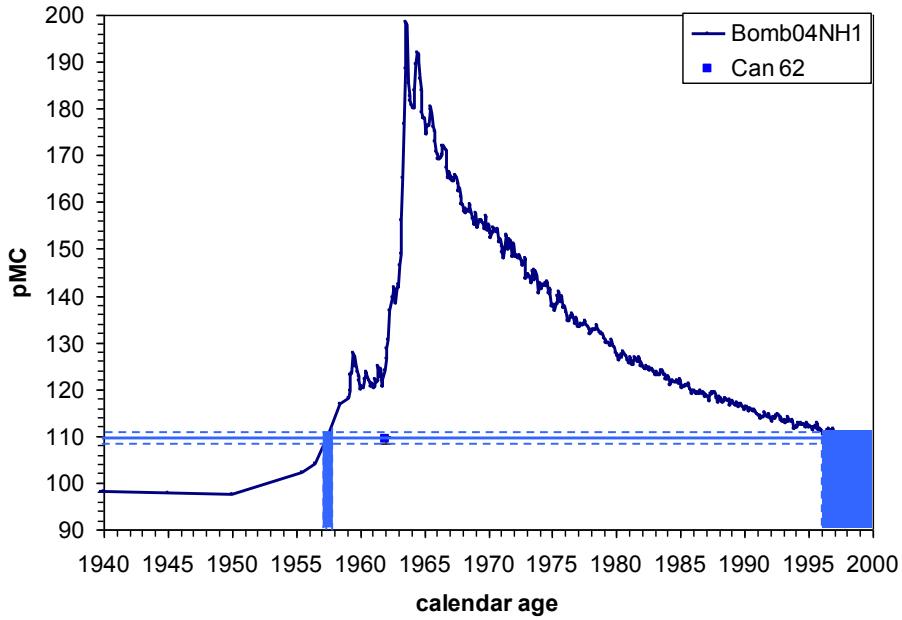

Fig 4.14 Example of calibration (sample "Can62") by intercepting the Bomb04NH1 curve with a horizontal line centred on the measured radiocarbon concentration. The measured radiocarbon concentration is also reported as a function of the painted year. With blue solid line the projection of the measured concentration is represented; the corresponding experimental uncertainty (1 sigma) is represented with a red dotted line.

Being the fibres of the measured canvas obtained from annual plants, the discrepancy between the year reported on the painting and the first calibrated time interval can be explained considering a reasonable time gap between the year when the plant was cut and when the canvas was really used by the artist. However, this is an intrinsic feature of dating an artefact by radiocarbon: the result will simply give us a *terminus post quem*, which can be not so important in case we are studying an archaeological or a geological issue, while can be really significant studyng a sample during the bomb peak period when ^{14}C concentration has rapidly changed.

Chapter 5
Case studies: dating a restored painting and identifying a fake

In this chapter, two case studies are shown. The first concerns the application of the new chloroform-based pre-treatment method, already described in chapter 3, on a restored painting of the early 20th century; as for the second case study, the identification of a forgery of an artwork supposed to be of the first half of the same century is presented. Both examples clearly prove how much important is the knowledge of the story of the studied artworks in order to choose the better protocol to use and to better interpret the results of radiocarbon measurements.

5.1 A restored painting

In paragraph 3.3.2, a new chemical pre-treatment protocol based on the use of chloroform was described. As its principal application, the removal of synthetic products employed in restoration was mentioned. After the preliminary tests performed on wood samples in order to verify the effectiveness of the pre-treatment, the new procedure was applied on a real case.

The case study is represented by an oil painting on canvas realized in 1918; the painting has undergone several restorations with the aim at consolidating the preparation and the painted layers. These operations are well documented in different technical reports. In all the cases, consolidation was performed by using the acrylic resin *Gustav Berger's Original Formula® 371* (Berger ethylene vinyl acetate, called BEVA 371 from now on). BEVA 371 is a product based on ethylenevinylacetate, paraffin and ketone resin, in a solution of aliphatic and aromatic solvents [wCt2011]. Since one of the principal characteristics of the consolidating resins is the capability to permeate into the materials, a simple physical treatment with a scalpel is not generally sufficient to remove them. In addition, their solubility

in organic solvents may decrease due to the polymerization processes, the natural ageing and the cross linking effect. However, as it is explained in chapter 3, the complete cleaning is mandatory since the acrylic resins contain dead carbon that can be the cause of an apparent ageing of the dated sample.

Concerning the analysed painting, a small sample from the rear edge of the canvas was collected (see Figure 5.1).

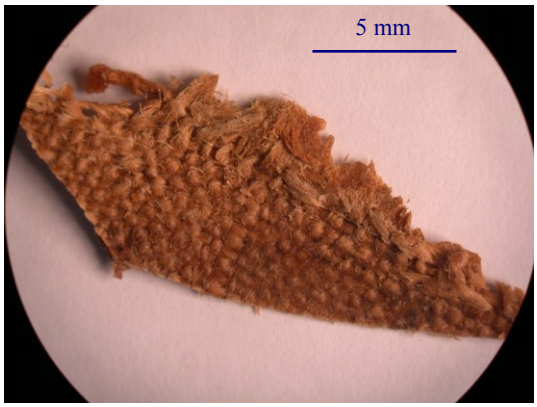

Fig. 5.1 Picture of the collected sample under the optical microscope: a brownish overlapping layer is visible.

Observing carefully the sample under an optical microscope, it is possible to notice that it is covered by a thick brownish layer. As in the case of the other textiles dated in this PhD work (see paragraph 4.3), the sample was analyzed by SEM in order to identify the raw material. The flax fibres were identified thanks to the characteristic elbows (see Figure 5.2).

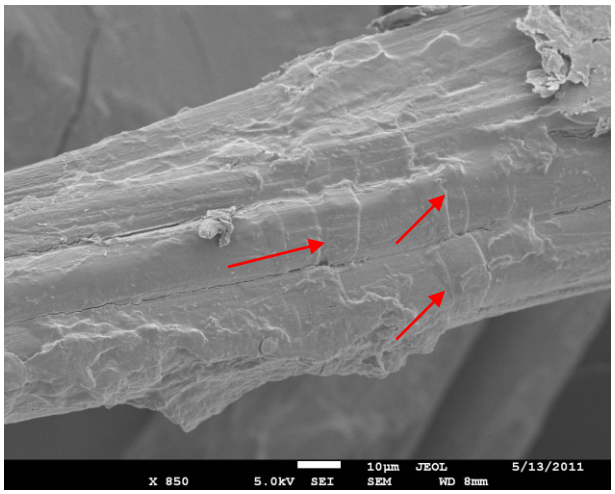

Fig. 5.2 SEM picture of the sample. The flax fibres are well identifiable thanks to the characteristic elbows (indicated with red arrows).

Considering the pre-treatment, the sample was cut in two fragments: one of them was treated just using the ABA standard protocol, the other using the new chloroform-based protocol (see paragraph 3.3.2 for all the operational details).

The measured radiocarbon concentrations and the corresponding radiocarbon ages are reported in Table 5.1.

Chemical protocol	**^{14}C conc. (pMC)**	**t_{RC} (years BP)**
ABA	79.31 ± 0.30	1862 ± 30
Chloroform_ABA	97.79 ± 0.39	179 ± 32

Table 5.1 Measured radiocarbon concentrations and corresponding radiocarbon ages for the fragment of the canvas sample treated either with or without chloroform.

As we can notice in Table 5.1, the experimental results show a large discrepancy between the concentration measured for the ABA-treated fragment and for the chloroform-treated sample. In particular, the sample prepared following the ABA protocol appears to be much older than expected, as it is still contaminated by a fraction of dead carbon. The ABA protocol is not clearly sufficient to remove the acrylic resin. On the contrary, the radiocarbon concentration measured in the fragment treated with the new protocol is in agreement with the expected value. Indeed, the radiocarbon age of 179 ± 32 years BP corresponds to the period during which a sample can be just classified as modern (1650 – 1950). This result is thus in agreement with the year written by the artist on the painting (1918).

The different effectiveness of the used pre-treatments has turned out to be evident looking at the radiocarbon data. As a further indication, during the different steps of the preparation, the sample was also analysed by the *Attenuated Total Reflection* (ATR) technique, to identify possible organic compounds mixed to the original fibre.

In the ATR spectrum of the original collected sample (see Figure 5.3), we observe different peaks that can be associated to paraffin and to ethylenevinylacetate, constituting the BEVA 371 consolidant used during the restorations. In particular (see also Table 5.2 for the references that can be found in the literature [Der1999]), we can notice:

- in the region between 3100 and 2800 cm^{-1}, the C-H stretching bands associated to the aliphatic group and the methyl group;
- the peak at 1730 cm^{-1} corresponding to the C=O stretching of the ester group;
- the peaks at 1450 and 1380 cm^{-1} corresponding to the CH_3 bending of the aliphatic group;

- in the region between 1300 and 900 cm^{-1}, the characteristic C-O stretching bands associated to the aliphatic group.

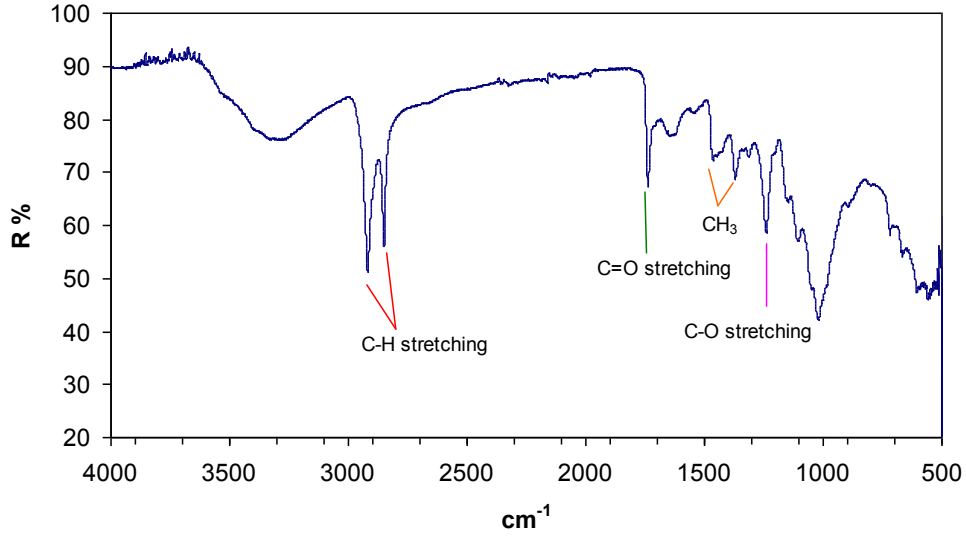

Fig. 5.3 ATR spectrum of the collected sample before any chemical pre-treatment. Some characteristic peaks corresponding to paraffin and ethylenevinylacetate, constituting the BEVA 371, are indicated.

	Wavenumber (cm^{-1})	**Bond**
Ethylenevinylacetate	3100-2800	C-H stretching
	1750-1650	C=O stretching
	1480-1300	C-H bending
	1300-900	C-O stretching
	750-700	C-H torsion
Paraffin	2962 and 2872	CH_3 stretching
	2926 and 2850	CH_2 stretching
	1450-1380	CH_3 bending
	1465	CH_2 bending
	730	CH_2 rocking

Table 5.2 Characteristic peaks visible in the IR region of ethylenevinylacetate and paraffin, components of BEVA 371.

In Figure 5.4, the spectra corresponding to the two fragments of the canvas sample treated with the two different protocols are presented.

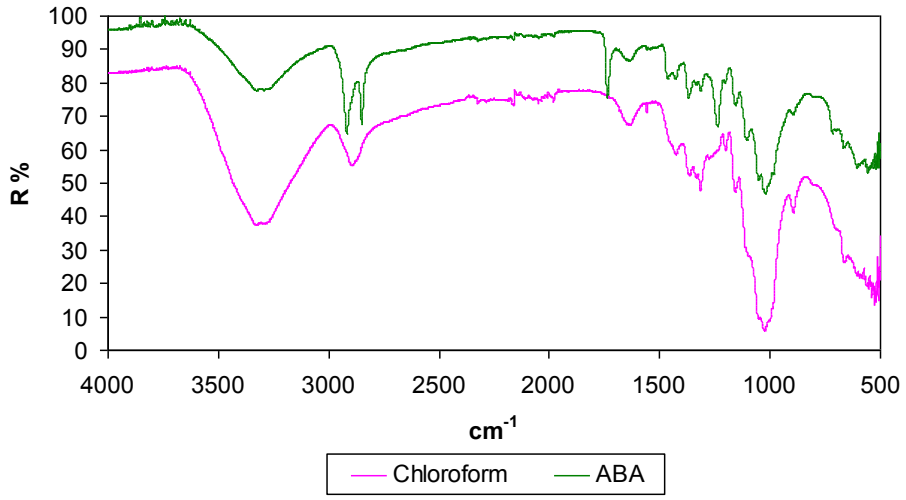

Fig. 5.5 Comparison between the ATR spectra of the fragments treated with ABA and the chloroform-based protocols.

As we can notice, the peaks relative to the consolidation product (see e.g. at 1730 cm^{-1} and in the region 3100-2800 cm^{-1}) are still present in the spectrum of the fragment treated with the ABA procedure while they are not visible in the spectrum of the fragment treated with chloroform, confirming the radiocarbon measurements. It is worth to notice that these ATR measurements helped us to verify the effectiveness of the different pre-treatments in a non-invasive way, so that the same analyzed samples were then combusted and graphitized to perform the AMS measurement.

To have a further confirmation of the use of BEVA 371 in the restorations, the material extracted with chloroform was also analyzed. All fractions were gathered and the resulting solution was evaporated under vacuum; the dried residue was dispersed in a KBr pellet (diameter 13 mm) which was analyzed in trasmission by FTIR. The FTIR spectrum of the residue is reported in Figure 5.5. The characteristic peaks of paraffin and ethylenevinylacetate, constituting the BEVA 371 consolidant are indicated.

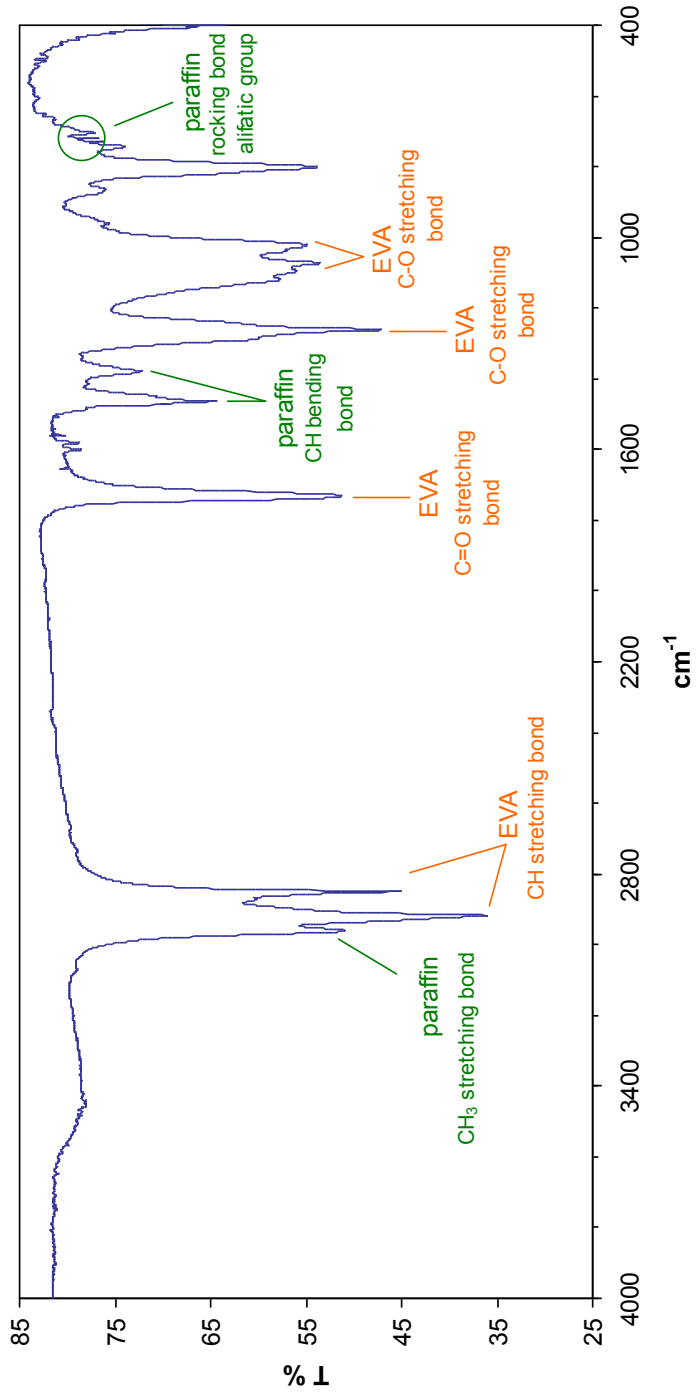

Fig. 5.4 FTIR spectrum of the residue extracted from the chloroform solution collected after the pre-treatment (EVA= ethylenvinilacetate).

In conclusion, the radiocarbon data combined with the results of ATR and FTIR analyses have highlighted the differences between the two different chemical pre-treatments and confirmed the effectiveness of the new chloroform-based sample preparation protocol.

5.2 A forgery of a contemporary artwork

In chapter 4, the radiocarbon measurements performed on paper and canvas samples have shown limits and advantages of the use of this isotope in dating recent objects and artworks. The capability to discriminate samples produced before and after 1950 can allow us also to unambiguously identify forgeries of paintings or artworks. Here, a case study is presented.

The artwork under investigation is a painting on canvas attributed to Fernand Léger (Argentan 1881- Gif-Sur-Yvette 1955). Regarding the artistic style, the painting seems to be part of the large corpus of works "*Contrastes de Formes*" composed since the late summer of 1913 until August 1914. In Figure 5.6 a picture of the painting is presented.

Fig. 5.5 Picture of the painting by F. Leger supposed to be dated back to 1913-1914 dated by radiocarbon.

According to historical documents, the painting was bought by Peggy Guggenheim during the 1960s at the John Berggruen Gallery (San Francisco). In 1970, the art critic Douglas Cooper raised suspicions about the authenticity of some works of Léger, such as some paintings of the group "*Contrastes de Formes*", in which this painting itself is included. In

1975, the Italian government inserted the Peggy Guggenheim collection into the list of the National Treasures, taking off any possibility to sell back any artwork. Anyway, in 1983, the art committee of the Solomon R. Guggenheim Foundation, owner of the collection, forbade to exihibit the painting, classifying it as a possible fake. Since then, the painting has remained kept at the Peggy Guggenheim Collection in Venice.

As far as the authentication of the painting is concerned, the pigments and the executive technique were studied in order to solve the doubts. Several non invasive and non destructive techniques (e.g. IR reflectography and X-rays radiography) and micro-destructive methods (e.g SEM) were used at the Archaeometry Laboratory of the Ferrara University [Min2008]. During these analyses, the comparison with artworks of the same period was also executed in order to recognize differences and similarities with respect to the painting of interest.

Because the analyses had highlighted some discrepancies with respect to the traditional technique used by Léger, we decided to also date by radiocarbon the painting, or at least the canvas used as support. Since Léger died in 1955, year from which the ^{14}C concentration has definitely increased due to the weapon nuclear tests (see paragraph 1.3.2), radiocarbon dating would have definitively solved the doubt of the authenticity.

In order to perform the dating, a fragment was collected from the rear edge of the canvas; the mass was about 20 mg. In Figure 5.6 a picture of the sample under optical microscope is reported.

Figure 5.6 View under the optical microscope of the canvas sample collected from the painting of Léger.

The sample was initially scratched using a scalpel and washed in ultrasonic bath for three times, 15 minutes each: the first bath was in a solution of ultra-pure water and acetone (1:1), the other two just in ultra-pure water. Afterwards, the fragment was dried in vacuum at 100 °C for 5 hours. At last, we treated the sample using the ABA standard protocol.

The measured radiocarbon concentration was:

- 129.05 ± 0.68 pMC.

Being the concentration bigger than 100 pMC, it is obvious that the painting is clearly later 1955. In particular, comparing the experimental measured concentration to the atmospheric data in the Bomb04NH1 curve (see Figure 5.8), we can notice that the curve is intercepted in three well separated time intervals (corresponding to 1959, 1962 and 1979-1980), which are subsequent to the death of the artist.

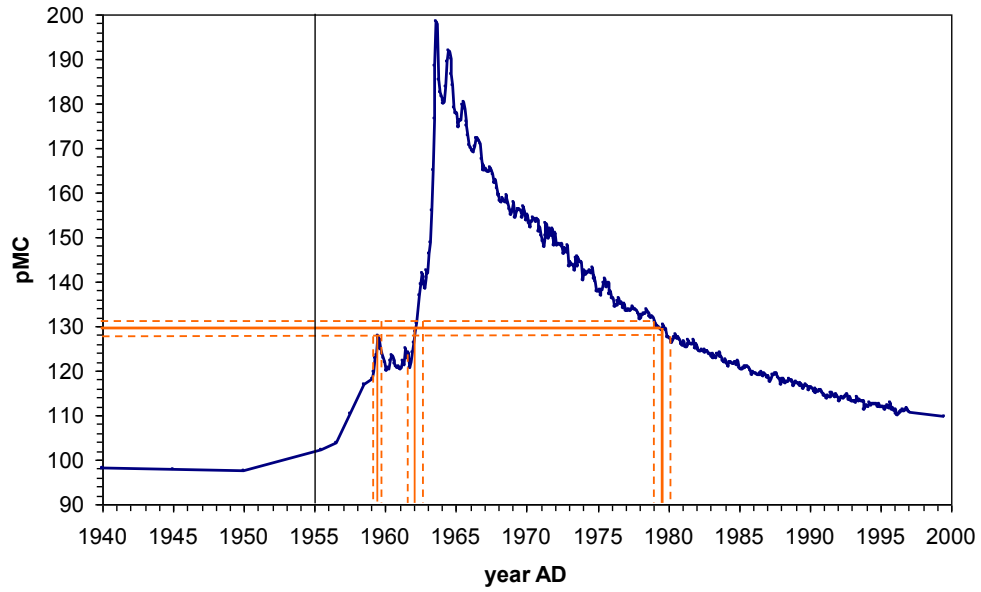

Figure 5.7 Calibration of the radiocarbon concentration by intercepting the Bomb04NH1 curve with a horizontal line centred on the measured value. With the vertical black line the year of the death of Léger is indicated; with orange solid line the projection of the measured concentration is represented; the corresponding experimental uncertainty (quoted at 1 sigma) is represented with orange dotted line.

Since during 1979-1980 the painting was surely part of the Guggenheim Collection, we can exclude this period. An ambiguity still remains because two other different time intervals are obtained as a result of the calibration, either 1959 or 1962. Moreover, as already explained in previous examples, this information is relative to the year when the plant was cut and not to the year when the canvas was really painted by the artist. However, considering that Léger died in 1955, the result of this measurement definitely demonstrates that this painting is a fake.

Eventually, it is evident how powerful radiocarbon can be for contemporary art authentication issues, i.e. for the identification of forgeries made in the last decades of the 20th century of artworks that are supposed to be of the first half of the same century.

Conclusions

In this thesis, I have discussed the possibility to date by radiocarbon samples collected from contemporary artworks, exploiting the so-called Bomb Peak. To this purpose, several samples of materials that are typically used in art, such as paper and canvas, were measured by ^{14}C-AMS (Accelerator Mass Spectrometry). Samples were taken from Italian newspapers published since the 1930s until present and from fine papers used in limited edition drawing prints, realized in the second half of the 20th century; canvas samples were collected from contemporary art paintings. The measured ^{14}C concentrations were compared to the expected concentrations estimated on the basis of the year indicated on each sample (i.e. the year of publishing/printing or the year signed by the painter), allowing us to highlight advantages and limits of the use of this dating method.

The experimental data have clearly pointed out that we can easily discriminate between samples of the first half and samples of the second half of the 20th century, giving us the possibility to use radiocarbon to solve authentication issues. Important differences between materials derived from long-living plants (dailies paper from wood) and from short-living plants (fine paper from cotton and canvas from cotton or flax) have been shown. In particular, concerning newspaper samples, comparing the experimental results with the reference Bomb04NH1 curve, lower ^{14}C concentrations than the atmospheric values were generally measured (in fact, in this case, the raw material is wood). Thus, even though we were able to perform radiocarbon measurements with a high precision, we have verified that, due to the characteristic manufacturing processes of paper, it is not possible to match each measured radiocarbon concentration to the corresponding calendar year in which the paper was produced. In the case of fine paper and canvas samples, we have noticed a general agreement between the measured radiocarbon concentrations and the expected values, although an offset of few years with respect to the expected date has been found. This discrepancy can be related to a reasonable time gap between the year when the plant, from which paper or canvas were manufactured, was cut and when these materials were really used.

All these radiocarbon measurements have been supported by a characterization of the samples by optical and electron microscopy (SEM), to study the state of preservation and the raw materials. This is very important to choose the better chemical protocol to apply for the sample preparation and to better interpret the radiocarbon results.

A big effort has been also put on the improvement of the experimental set-up. One of the hardware developments concerned the installation of a new graphitization line; thanks to this upgrade, the radiocarbon concentrations measured in blank samples were satisfactory. In addition, thanks to the new silicon photodiode installed as rare isotope detector on the AMS beam line, a remarkable improvement of the energy resolution was achieved, paving the way also to the measurement of rare isotopes other than ^{14}C. Moreover, two new chemical pre-treatment protocols were tested: these protocols were especially dedicated to deteriorated cellulose-based materials (alpha cellulose extraction protocol) and to restored artworks (chloroform-based protocol). Besides radiocarbon measurements on several test samples, the effectivenes of these new pre-treatments was also confirmed by using other techniques, i.e. FTIR and ATR. Since these techniques are non destructive (ATR) or require just a very small quantity of sample (FTIR), their use during the sample preparation steps to verify the applied protocols can be proposed as a routine practice.

The results achieved with this work have demostrated to be very important in view of application to some real cases. The ^{14}C measurements performed on a canvas sample collected from a restored painting have confirmed the effectiveness of the new chloroform-based sample preparation protocol. The dating of a painting attributed to F. Léger, that has been measured to be a fake, has shown how powerful radiocarbon can be for contemporary art authentication issues, i.e. for the identification of forgeries made in the last decades of the 20th century of artworks that are supposed to be of the first half of the same century.

The research developed in these three years have shown advantages and limits of radiocarbon dating in studying of atrworks of the 20th century. In particular, we have proved that it is possible to solve authentication issues especially for samples obtained from annual plants. This important result can be very useful for the art critics, the curators of the museum and the art merchants. It is obvious that the radiocarbon measurements and the other scientific techniques have always to be supported by the knowledge of other independent information concerning for example the story of the sample to be dated.

Bibliography

[Anc2008] K.J. Anchukaitis et al., *Consequence of a rapid cellulose extraction technique for oxygen isotope and radiocarbon analyses*, Analytical Chemistry 80, p. 2035-2041

[Aws1986] R. Awsiuk and M.F. Pazdur, *Regional Suess effect in the Upper Silesia urban area*, Radiocarbon 28 (2A), p. 655-660

[Bow1990] S. Bowman, *Radiocarbon dating*, British Museum Publication Ltd (1990)

[Bru2001] F. Bruhn et al., *Chemical removal of conservation substances by Soxhlet type extraction*, Radiocarbon 43 (2A), p. 229-237

[Cra1954] H. Craig, *Carbon-13 in plants and the relationships between carbon-13 and carbon-14 in nature*, Journal of Geology 62 (2), p. 115-149

[Cop1994] T.B. Coplen, *Reporting of stable hydrogen, carbon and oxygen isotopic abundances*, Pure Applied Chemistry 66, p. 273-276

[Der1995] V. Dergacev and V. Christyakov, *Cosmogenic radiocarbon and cyclical natural processes*, Radiocarbon 37, p. 417-424

[Fed2007] M.E. Fedi, *The ^{14}C AMS facility at LABEC, Florence*, NIM (B) 259, p.18-22

[Fin1993] R.C. Finkel and M. Suter, *Advances in analytical geochemistry*, vol. 1, p. 1-114

[God1962] H. Godwin, *Half-life of radiocarbon,* Nature 195, p.984

[Hor2010] V. Horie, *Materials for conservation. Organic consolidants, adhesives and coatings (second edition)*, Elsevier Ltd

[Hua2004] Q. Hua and M. Barbetti, *Review of tropospheric bomb ^{14}C data for carbon cycle modeling and age calibration purpose*, Radiocarbon 46, p. 1273-1298

[Jer2010] R.J. Jerusik, *Fungi and paper manufacture*, Fungal Biology Reviews 24, p. 68-72

[Kaw2007] H. Kawamura et al, *^{14}C measurements of tree rings of a Japanese cedar during 1945 to 2000 and core sampling for environmental studies*, Radiocarbon 49 (2), p. 1045-1053

[Kei1972] B.Keish and H. Miller, *Recent art forgeries: detection by carbon-14 measurements*, Nature 240, p. 491-492

[Kil1997] L.R. Kilius et at., *Ion source design criteria for AMS*, NIM (B) 123, p. 5-9

[Kno1979] G.F. Knoll., *Radiationdetection and measurement*, J. Wiley and Sons

[Kor1980] S.A Korff and R.B. Mendell, *Variations in radiocarbon production in the earth's atmosphere*, Radiocarbon 22, p. 159-165

[Kre2004] W. Kretschmer et al., *The mystery of Persian mummy: original or fake?*, NIM (B) 223-224, p. 672-675

[Laz2007] B. Lazzeri, *Studio di un rivelatore per lo studio di interferenze isobariche in misure AMS* , Tesi di laurea a.a. 2006-2007

[Lev1989] I.Levin et al, *The continental european Suess Effect*, Radiocarbon 31, p. 431-440

[Lev2000] I.Levin et V. Hesshaimer, *Radiocarbon- A unique tracer of global carbon cycle dynamics*, Radiocarbon 42 (1), p. 69-80

[Lib1960] W. Libby, *Radiocarbon Dating*, Nobel lectures, p. 593-610

[Lop2011] L. Lopez-Polin, *Possible interferences of some conservation treatments with subsequent studies on fossil bone: a conservator's overview*, Quaternary international, doi:10.1016/j.quaint.2011.07.039

[Man1983] W.B. Mann, *An international reference material for radiocarbon dating*, Radiocarbon 25 (2), p. 519-527

[Min2008] F. Minarelli., *I "Contrastes de formes" di Fernand Léger: diagnostica per immagini alla Peggy Guggenheim Collection*, Tesi di laurea a.a.2007-2008

[McC2010] G.S.O. McCullagh et al., *Radiocarbon dating of individual amino acids from archaeological bone collagen*, Radiocarbon 52 (2-3), p. 620-634

[McG2004] E.J. McGee et al., *Recent chronologies for tree rings and terrestrial archives using ^{14}C bomb fallout history*, Geochimica et Cosmochimica Acta 68 (11), p. 2509-2516

[Paw2000] S.Pawelczyk and A.Pazdur, *$\delta^{13}C$ in tree rings α-cellulose. A methodology of measurements and interpretation: state of the art*, Geochronometria 18, p. 15-18

[Paw2004] S.Pawelczyk and A. Pazdur, *Carbon isotopic composition of tree rings as a tool for biomonitoring CO_2 level*, Radiocarbon 46 (2), p. 701-719

[Paz2005] A. Pazdur et al, *Carbon-13 in α-cellulose of oak latewood (Jedrejow, Southern Poland) during the Maunder Minimum*, Geological Quarterly 49, p. 165-172

[Pea1986] G.W. Pearson and M. Stuiver, *High-precision calibration of the radiocarbon time scale, 500-2500 BC*, Radiocarbon 28 (2B), p.839-862

[Qua2005] G. Quarta et al, *New bomb pulse radiocarbon records from annual tree rings in the northern hemisphere temperate region*, Radiocarbon 47 (1), p. 27-30

[Rei2009] P.J. Reimer et al., *IntCal09 and Marine09 Radiocarbon age calibration curves, 0-50.000 years cal BP*, Radiocarbon 51 (4), p. 1111-1150

[Rin2005] K.T. Rinne et al, *On the purification of α-cellulose from resinous wood for stable isotope (N, C and O) analysis*, Chemical Geology 222, p. 75-82

[Ruf2010] M. Ruff et al., *Gaseous radiocarbon measurements of small samples*, NIM (B) 268, p. 790-794

[Sco2007] E.M. Scott et al, *A report on phase 1 of the 5th International Radiocarbon Intercomparison (VIRI)*, Radiocarbon 49 (2), p. 409-426

[Sco2010] E.M. Scott et al, *The Fifth International Radiocarbon Intercomparison (VIRI): an assessment of the laboratory performance in stage 3*, Radiocarbon 52 (2-3), p. 859-865

[Spa2008] K.L. Spalding, *Dynamics of fat cell turnover in humans*, Nature 453, p. 783-787

[Ste1983] R.S. Sternberg and P.E. Damon, *Atmospheric radiocarbon: implications for the geomagnetic dipole moment*, Radiocarbon 25, p. 239-248

[Stu1977] M. Stuiver and H.A. Polach, *Reporting of ^{14}C data*, Radiocarbon 19, p. 355-363

[Stu1986] M. Stuiver and G.W. Pearson, *High-precision calibration of the radiocarbon time scale, AD 1950- BC 500*, Radiocarbon 28 (2B), p.805-838

[Sue1986] H. Suess, *Secular variations of cosmogenic ^{14}C on earth: their discovery and interpretation*, Radiocarbon 28, p. 259-265

[Tac2010] F. Taccetti et al, *A beam Profile Monitor for rare isotopes in Accelerato Mass Spectrometry: preliminary measurements*, Radiocarbon 52, p. 272-277

[Tal2011] S. Talamo, *A comparison of bone pretreatment methods for AMS dating of samples >30.000 BP*, Radiocarbon 53 (3), p. 443-449

[Tun1998] C. Tuniz et al., *Accelerator Mass Spectrometry. Ultrasensitive technique for global science*, CRC Press LLC

[Tun2004] C. Tuniz et al., *Sherloc Holmes counts the atoms*, NIM (B) 213, p. 469-475

[Wei1997] I.A. Weinstock et al., *A new environmental benign technology for transforming wood pulp into paper. Engineering of polyoxometalates as catalysts for multiple processes*, Journal of molecular catalyst A: Chemical 116, p. 59-84

[Wil2000] E.M. Wild et al., *^{14}C dating with the bomb peak: an application to forensic medicine*, NIM (B) 172, p. 994-950

[wAt2000] http://atom.kaeri.re.kr

[wCt2011] http://www.ctseurope.com/

[wHi99] www.c14dating.com

[wFa2011] http://www.fas.org/nuke/control/npt/

[wIa2011] http://www.iaea.org/

[wRo2011] http://www.rohmhaas.com

[YOh2005] S. Youn Oh et al., *FTIR* analysis of cellulose treated with sodium hydroxide and carbon dioxide, Carbohydrate research 340, p417-428

[Zav2007] D. Zavattaro et al., *Recent documents dating: an approach using radiocarbon technique*, Forensic science international 167, p. 160-162

[Zop2004] U. Zoppi et al., *Forensic applications of ^{14}C bomb pulse dating*, NIM (B) 223-224, p. 770-775